ELSEVIER

Chemical Geology 157 (1999) 119–146

CHEMICAL GEOLOGY
INCLUDING
ISOTOPE GEOSCIENCE

Crust–mantle interaction induced by deep subduction of the continental crust: geochemical and Sr–Nd isotopic evidence from post-collisional mafic–ultramafic intrusions of the northern Dabie complex, central China

Bor-ming Jahn [a,*], Fuyuan Wu [a,b], Ching-Hua Lo [c], Chin-Ho Tsai [d]

[a] *Géosciences Rennes, Université de Rennes 1, Campus de Beaulieu, 35042 Rennes Cedex, France*
[b] *Department of Geology, Changchun University of Earth Sciences, Changchun 130061, China*
[c] *Department of Geology, National Taiwan University, 245 Choushan Rd., Taipei 10770, Taiwan*
[d] *Department of Geological and Environmental Sciences, Stanford University, Stanford, CA 94305, USA*

Received 20 May 1998; revised 2 December 1998; accepted 2 December 1998

Abstract

Interaction of deeply subducted continental blocks with the upper mantle peridotite is a likely process, but it has never been demonstrated. New geochemical and isotope tracer analyses of post-collisional mafic–ultramafic rocks from the Dabie terrane in central China show that they could have been generated by melting of such metasomatized mantle as a result of crust–mantle interaction. Isotopic dating using different techniques (Rb–Sr, Sm–Nd and Ar–Ar) has established that these mafic–ultramafic rocks were emplaced post-tectonically in early Cretaceous ($\approx$ 120–130 Ma), nearly contemporaneous with the massive intrusions of granitic plutons. They did not form as part of the early Paleozoic arc complex, nor did they undergo UHP metamorphism at about 220 Ma. The strong enrichment of light rare earth elements (REE) and the highly negative $\varepsilon_{Nd}(T)$ values (about -15 to -20) for all mafic and ultramafic rocks indicate their derivation from an enriched mantle source. Significant negative Nb anomalies observed in the spidergrams and other 'crustal' signatures of these rocks suggest an important role of continental material in their petrogenesis. We interpret that the singular geochemical and isotopic characteristics witness a post-collisional interaction between the subducted ancient crust (Yangtze craton) and the mantle peridotite (asthenosphere). Partial melting of such metasomatized mantle produced the basic magmas, in response to the same thermal pulse that was responsible for the massive Cretaceous granitic intrusions and resetting of some isotopic clocks in UHP metamorphic rocks. Taking into consideration all geochemical and isotopic constraints, a tectonic model is presented with emphasis on the post-collisional crust–mantle interaction and possible heat sources required for massive Cretaceous granitic intrusions. We also advocate that the digestion of deeply subducted continental blocks in the upper mantle may represent an efficient way of crustal recycling when dealing with the problem of continental growth and destruction.

Keywords: Dabie terrane; UHP terrane; Continental subduction; Mafic–ultramafic intrusion; Crust–mantle interaction; Age dating; Sr–Nd isotopes

* Corresponding author. Tel.: +33-99-28-60-83; fax: +33-299-28-67-72; e-mail: jahn@univ-rennes1.fr

0009-2541/99/$ - see front matter
PII: S0009-2541(98)00197-1

1. Introduction

The Dabie Mountains and the Su-Lu region in central China are known to contain the largest distribution of ultrahigh pressure metamorphic (UHPM) rocks in the world. They are parts of the Qinling–Dabie orogen formed by collision between the Sino-Korean and Yangtse cratons (Fig. 1). Coesite-bearing rocks (mainly eclogites) are widely distributed in the two terranes which are truncated by the Tanlu Fault and offset by about 500 km. The preservation of UHP minerals has inspired different models to explain the genesis of extreme crustal thicknesses and the mechanisms for subsequent unroofing of the UHPM rocks (e.g., Chopin, 1984; Anderson et al., 1991; Avigad, 1992; Michard et al., 1993; Davis and von Blanckenburg, 1995; Hacker et al., 1995, 1998). In the absence of good constraints from geochemical, isotopic and age data for different lithotectonic units, numerous tectonic models have been proposed (Mattauer et al., 1985, 1991; Okay and Sengör, 1992; Xu et al., 1992; Yin and Nie, 1993; Li, 1994; Wang, 1996). It appears that the greatest controversy to date concerns the primary ages for different lithological units, the nature of eclogite protoliths, their relation with the associated ultramafic rocks and enclosing granitic gneisses (or the 'in-situ' vs. 'foreign' hypothesis), the areal extent of the UHPM rocks, and their mode of exhumation. A comprehensive study of geochemical and Nd–Sr isotopic characteristics for different types of eclogites and their associated ultramafic rocks from the Dabie and Su-Lu UHP terranes was presented by Jahn (1998) and the data were used to constrain (1) the petrogenesis of the coesite-bearing eclogites and associated ultramafic rocks, and (2) the tectonic evolution of the Qinling–Dabie collisional belt.

Subduction of continental blocks such as shown in the Dabie UHP terrane may have a direct implication for crustal recycling and a likely consequence of crust–mantle interaction. We have 'discovered' that post-collisional mafic intrusions in the northern Dabie complex (NDC) of the Dabie terrane possess highly unusual geochemical and isotopic characteristics that may be used to argue for the effect of crust–mantle interaction. The purposes of this paper are: (1) to present new age information for the magmatic intrusions using Rb–Sr, Sm–Nd and Ar–Ar isotopic analyses on whole-rock samples and their mineral constituents, (2) to use geochemical and Sr–Nd isotope tracers to constrain the petrogenetic processes of these rocks, and (3) to discuss tectonic implications for the Dabie collisional orogen.

2. General geology of the NDC

The general geology of the Su-Lu and Dabie UHP metamorphic terranes has been described in numerous recent publications (Eide, 1995; Wang et al., 1995; Cong, 1996; Hacker et al., 1996; Liou et al., 1996; among others). Briefly, the Dabie terrane is composed of three major petrotectonic units: (1) the northern Dabie orthogneiss complex, (2) the central Dabie UHP metamorphic complex, and (3) the southern Dabie HP blueschist/greenschist terrane. They are bounded in the south by a Triassic foreland fold-thrust belt and in the north by a greenschist facies meta-sedimentary unit, the Foziling Group, which is composed of several kilometers of quartzite and biotite–muscovite quartz schist (RGS Anhui, 1987), and has been commonly interpreted as flysch deposits or as passive continental apron deposits of the Yangtze craton (Okay et al., 1993). The Foziling Group is equivalent to the North Huaiyang Flysch Belt used by other authors. All three petrotectonic units are intruded by Cretaceous granitoids.

The NDC (Fig. 1) consists dominantly of granitic gneisses of TTG compositions (trondhjemite–tonalite–granodiorite; Jahn et al., 1994, 1995; Wang et al., 1996) and subordinate migmatite, amphibolite, garnet granulite, marble and some conspicuous trains of mafic–ultramafic rocks (Wang and Liou, 1991; Okay et al., 1993; Wang et al., 1996; Zhang et al., 1996). Eclogitic rocks have not been undisputably identified, but UHP metamorphism has been inferred based on some relic mineralogy (Tsai and Liou, 1997). The bulk of the NDC has been interpreted as a Cretaceous extensional-magmatic complex (Hacker et al., 1995, 1998). The most deformed zone is within greenschist-facies mylonites and ultramylonites along the Xiaotian–Mozitang detachment fault at the northern topographic limit of the Dabie Mountains (Hacker and Wang, 1995). The common gneisses show banded texture and are strongly foli-

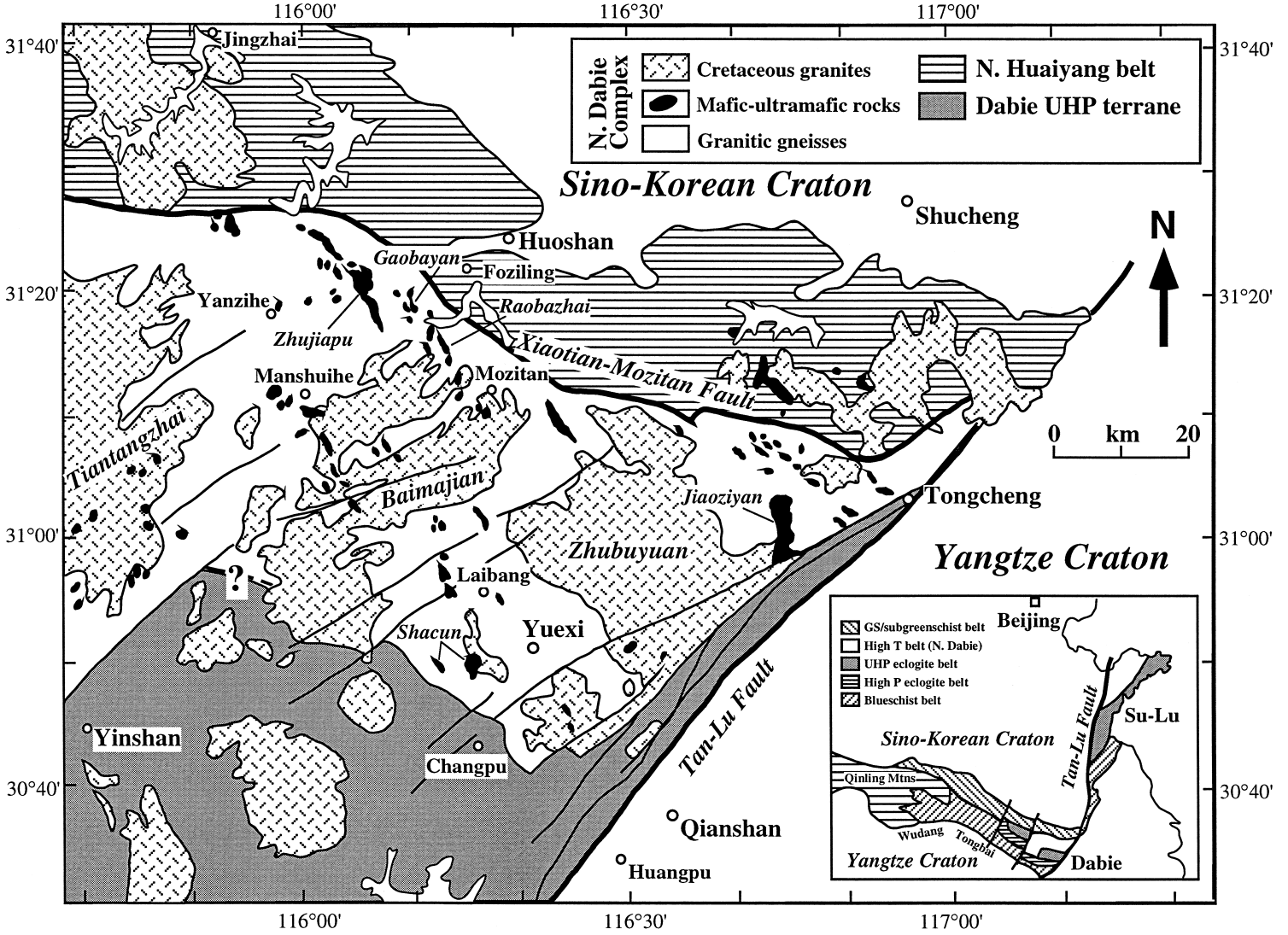

Fig. 1. Geologic sketch map of the NDC. Sampling localities are roughly indicated by the names of Shacun, Zhujiapu and Jiaoziyan.

ated, medium-grained, frequently porphyroblastic, containing enclaves of amphibolites. The banding in the gneisses plunges to the north and northwest at 30–60° angle. Migmatitic gneisses show partial melting structures and the zones of melting also form ductile shear zones suggesting syndeformational partial melting (Okay et al., 1993). The NDC is in general characterized by amphibolite facies metamorphism and partial melting. However, the presence of mafic granulites at several localities suggests that the NDC may have reached granulite facies metamorphism that was strongly overprinted by the amphibolite facies and later thermal event when massive Cretaceous granites were emplaced. Furthermore, preservation of garnet growth zoning in a felsic granulite from Luotian (NW of Yinshan, out of map in Fig. 1) led Chen et al. (1998) to suggest a short residence time for the granulite at peak metamorphism and thus a rapid tectonic uplift history.

Because of the intense deformation and thermal recrystallisation prior to and during the Cretaceous granitic intrusion, the metamorphic complex has been interpreted as a thermally overprinted subduction complex (Wang and Liou, 1991; Okay and Sengör, 1992; Maruyama et al., 1994), as a Paleozoic Andean magmatic arc complex (Wang et al., 1996), as a metamorphic ophiolite melange complex (Xu et al., 1992, 1994, 1995), as a Cretaceous magmatic belt formed during large-scale extension (Hacker et al., 1995), or as the Sino-Korean hangingwall during Triassic subduction for the formation of the UHP units to the south (Zhang et al., 1996).

The ages of the protolith(s) for most lithologic units are not yet determined. Our Sm–Nd isotopic analyses of granitic gneisses give T_{DM} model ages of 1.5–1.8 Ga which provide the upper limit for the ages of their protoliths. Biotite and hornblende from the orthogneiss complex yielded Ar–Ar ages of 120–130 Ma (Hacker and Wang, 1995) and biotite–plagioclase–whole-rock Rb–Sr isochrons gave about 115 Ma (Potel and Jahn, unpublished). These ages are similar to the cooling ages of the widespread Cretaceous granitic intrusions, and were once believed to reflect reheating by post-collisional magmatic/extensioanl event (Hacker and Wang, 1995). The latest zircon age studies (Xue et al., 1997; Hacker et al., 1998) suggest that the bulk of the NDC is a Cretaceous magmatic complex, and the pre-Cretaceous 'basement rocks', represented by garnet granulite with minor marble and ultramafic rocks, are only scraps of the Yangtze craton that survived the deep subduction (Hacker et al., 1998). This interpretation is quite revolutionary. A further discussion will be presented later (Section 4.4).

Mafic and ultramafic rocks (gabbros and pyroxenites) are widely distributed and form several linear alignments (Fig. 1). Most of them represent a post-tectonic intrusive complex, comprising more than 130 composite bodies of variable dimensions ranging from 0.2×0.5 to 2×8 km^2 (Zhang et al., 1996). However, in the past these rocks have been variably, and erroneously, considered as ophiolite suites or subducted Tethys oceanic lithosphere (Liu and Hao, 1989; Xu et al., 1992; Okay, 1993; Xu et al., 1995), or as components of the arc complex formed in early Paleozoic and prior to the continental collision that produced the Qinling–Dabie orogen (Li et al., 1989a,b, 1993; Wang et al., 1996). The intrusive mafic–ultramafic rocks are generally undeformed, show no or little sign of metamorphism, and display distinct cumulate textures and intrusive relations with country gneisses. Gabbros from Shacun (Fig. 1) have a pegmatitic texture with grain size up to 2 cm. At Zhujiapu (Fig. 1), coarse-grained pyroxenite is cut by fine-grained gabbro and anorthosite dikes.

Alpine-type ultramafic blocks are relatively rare and the most representative is the Raobazhai 'massif' near Mozitan (Fig. 1). This 'massif', or better termed as tectonic slice based on unpublished Chinese drilling reports, consists mainly of Cr-spinel harzburgite, dunite, and lherzolitic mylonite; it is in fault contact with the surrounding migmatitic orthogneisses (Xu et al., 1994; Tsai and Liou, 1997). Minor plagioclase hornblendite dikes crop out near the rim of this massif. The entire massif was definitely not emplaced as intrusive body. It has been recrystallized in granulite- to amphibolite-facies conditions (700–800°C), presumably isofacial with the surrounding gneisses (Tsai et al., 1998). A higher pressure precursor stage is possible, but direct evidence for UHP is still lacking. The Raobazhai massif, with its Sm–Nd metamorphic age of ≈ 240 Ma and $\varepsilon_{Nd}(T) \approx -3$ (Li et al., 1993), is genetically unrelated to the rocks studied herein.

It should be noted that mafic–ultramafic intrusions are not limited to the NDC. They also occur in

the North Huaiyang Belt to the north and in the southern Dabie HP terrane (RGS Anhui, 1987). In addition to the gneiss complex and mafic–ultamafic massifs, the NDC contains voluminous Cretaceous granitic intrusions. Geochemical and Sr–Nd–Pb isotopic tracer studies indicate that these granites were derived from remelting of old (mid-Proterozoic?) continental crust, probably at a lower crustal level (Zhou et al., 1992, 1995b; Zhang et al., 1995; Xie et al., 1996; Chen and Jahn, 1998).

3. Analytical procedures

Four gabbro, three diorite and one olivine pyroxenite samples from the NDC have been analysed for chemical and Sr–Nd isotopic compositions. Petrographic descriptions for the analyzed samples are given in Appendix A.

3.1. Elemental abundances

Whole-rock powdered samples were prepared in agate mortars in order to minimize potential contamination of transition metals. Mineral separates were done mainly by magnetic separation and further purified by hand-picking. Major and trace element contents (except REE) were measured by XRF using a Philips PW1480 spectrometer in Rennes. Analytical uncertainties are $\pm 1\%$ to 3% for major elements; $\pm 5\%$ for trace elements ≥ 20 ppm and $\pm 10\%$ for those ≤ 20 ppm. REE abundances were determined by the isotope dilution method using a single-collector Cameca TSN-260 mass spectrometer. Uncertainties are $\pm 3\%$ for La and Lu and $\pm 2\%$ for other REE's.

3.2. Sr–Nd isotopic analyses

The analytical procedures for isotopic analyses are the same as reported earlier (Chavagnac and Jahn, 1996; Jahn et al., 1996). Analytical precisions, Sr–Nd isotope standard and normalization values, and blank levels can be found in the footnotes of data tables. The decay constants (λ) used in age computation are: $^{87}Rb = 0.0142\ Ga^{-1}$ and $^{147}Sm = 0.00654\ Ga^{-1}$. Model ages ($T_{DM}$) were calculated using the following equation assuming a linear Nd isotopic growth of the depleted mantle reservoir from $\varepsilon_{Nd} = 0$ at 4.56 Ga to $\varepsilon_{Nd} = +10$ at the present:

$$T_{DM} = 1/\lambda \ln\left\{\left[\left(^{143}Nd/^{144}Nd\right)_s - 0.51315\right] / \left[\left(^{147}Sm/^{144}Nd\right)_s - 0.2137\right]\right\}$$

Rb–Sr and Sm–Nd isochron calculations were done using the regression programs of ISOPLOT (Ludwig, 1990). Input errors used in age computations are: $^{147}Sm/^{144}Nd = 0.2\%$, $^{143}Nd/^{144}Nd = 0.005\%$; $^{87}Rb/^{86}Sr = 2\%$, and $^{87}Sr/^{86}Sr = 0.005\%$. Analytical precisions of isotope ratio measurements are given as ± 2 standard errors ($2\sigma_m$), whereas the quoted errors in age and initial isotopic ratios represent ± 2 standard deviations (2σ).

3.3. Ar–Ar analyses

Mineral separation was achieved using a combination of magnetic, heavy liquid, and hand-picking techniques. The 80–120 mesh fractions were selected for argon isotope analyses. Weighed aliquots of mineral separates were wrapped in aluminum foil packets and stacked in an aluminum canister with the irradiation standard LP-6 biotite (Odin et al., 1982) to monitor the neutron flux. They were irradiated in the VT-C position of the THOR Reactor at Tsing-Hua University (Taiwan) for 8 h with a fast neutron flux of 1.566×10^{13} n/(cm^2 s). After irradiation, the samples were degassed in steps from 550 to 1200°C with a 30 min/step heating schedule, and the purified gas was analyzed with a VG3600 mass spectrometer at National Taiwan University. The concentrations of ^{36}Ar, ^{37}Ar, ^{38}Ar, ^{39}Ar and ^{40}Ar were corrected for system blank, radioactive decay of nucleogenic isotopes, and minor interference reactions involving Ca, K and Cl. The detail analytical and correction techniques have been discussed by Lo and Lee (1994).

The $^{40}Ar/^{39}Ar$ data were plotted on apparent age spectrum and $^{36}Ar/^{40}Ar$–$^{39}Ar/^{40}Ar$ isotope correlation diagrams. The integrated dates were calculated from the sum total of the peak heights and their errors from the square root of the sum of squares of the peak height errors for all temperature steps. The

plateau dates were calculated by the same approach but utilizing only those dates on the plateau. A 'plateau' is defined if: (1) there are at least four successive temperature steps with dates that fall within 2σ of the average, (2) the gas fraction for the plateau steps should consist of more than 50% of total ^{39}Ar released, (3) the plateau steps should yield a linear array on the isotope correlation (or isochron) diagram with an acceptable goodness of fitting parameters, i.e., mean square of weighted deviates (hereafter MSWD), (4) the $^{40}Ar/^{36}Ar$ intercept value obtained from the isotope correlation (or isochron) diagram should not be significantly different from the atmospheric ratio (i.e., $^{40}Ar/^{36}Ar = 295.5$), and (5) the plateau date and the intercept (isochron) date on the isotope correlation diagram should be concordant (Lanphere and Dalrymple, 1978). In the isotope correlation diagram, the regression line yields two intercepts. The inverse of $^{39}Ar/^{40}Ar$ intercept produces a so-called intercept date, whereas the inverse of the $^{36}Ar/^{40}Ar$ intercept indicates the composition of a non-radiogenic argon component. The cubic least-square fitting scheme outlined by York (1969) was employed in regressing the data. The Ca/K and Cl/K ratios for gas from each temperature step were derived from the measured $^{37}Ar_{Ca}/^{39}Ar_K$ and $^{38}Ar_{Cl}/^{39}Ar_K$ ratios according to the relationships $Ca/K = 1.78 \times {}^{37}Ar_{Ca}/^{39}Ar_K$ and $Cl/K = 0.52 \times {}^{38}Ar_{Cl}/^{39}Ar_K$ for the samples irradiated at the THOR Reactor (Lo and Lee, 1994).

4. Results and discussion

4.1. Geochemical characteristics

The results of major and trace element analyses are given in Table 1. Some notable geochemical features are summarized below.

(1) Fig. 2a and b shows the variation of major and trace elements as a function of mg values, which serve as a rough index of magmatic differentiation. The overall variations in major elements (Fig. 2a) are consistent with the change of mg values except for a high-Mg diorite (BJ93-23) from Shacun and a gabbro or gabbroic diorite from Zhujiapu (mg = 43).

(2) BJ93-23 appears to have a composition similar to that of a high-Mg andesite or boninite formed by wet melting of mantle peridotite (e.g., Tatsumi and Eggins, 1995). However, this sample does not represent an andesitic liquid, but is an amphibole cumulate complementary to the light-colored diorite (BJ93-22) (see Appendix A).

(3) All chondrite-normalized REE patterns are highly enriched in light REE's (Fig. 3). They are completely different from those of ocean floor basalts (N-MORB) which are characterized by LREE depletion. Any assignment of the mafic–ultramafic rocks as ophiolite suites (e.g., Xu et al., 1994) must be erroneous. The REE patterns of gabbros and diorites (except the high-Mg one) from Shacun are comparable with those of alkali basalts and their differentiates (e.g., trachyandesites), but there are sufficient differences between them in terms of total alkalis, TiO_2, P_2O_5 and Nb abundances. The pyroxenite (BJ95-03) and fine-grained gabbro (BJ95-04) from Zhujiapu (Table 1; Fig. 3) appear to have a genetic relationship, with pyroxenite as Cpx–Opx cumulate from a more primitive gabbroic magma (not sampled) whereas the fine-grained gabbro (or diorite) represents a differentiated liquid (very low Ni and Cr contents of 8 and 6 ppm, respectively; data confirmed by duplicate analyses) from the same magma but was enriched in Al_2O_3 ($\approx$ 20%), Zr ($\approx$ 500 ppm), Sr ($\approx$ 1500 ppm) and Ba ($\approx$ 2400 ppm). In fact, sample BJ95-04 is characterized by high modal abundance of plagioclase and accessory apatite and

Notes to Table 1:
(1) Major and trace elements analyzed by XRF (Philips PW1480 spectrometer) in Rennes.
(2) Uncertainties (XRF): $\pm$1% to 3% for major elements; $\pm$5% for trace elements $\geq$ 20 ppm and $\pm$10% for those $\leq$ 20 ppm.
(3) Uncertainties (ID): $\pm$3% for La and Lu, and $\pm$2% for other REE.
(4) mg value = molecular proportion of MgO/(MgO + FeO), assuming 90% of total iron oxides as FeO. mg value = [MgO]/{[MgO] + 0.505 ([FeO] + 0.9 [Fe_2O_3])}, if FeO and Fe_2O_3 are reported separately.
(5) REE of sample 95DB-13P were analyzed by J.A. Barrat by ICP-MS in Grenoble (May, 1998).

Table 1
Chemical compositions of mafic–ultramafic bodies—the NDC

Sample no.	BJ93-10	BJ93-11	BJ93-21	BJ93-22	BJ93-23	BJ95-03	BJ95-04	95DB-13P	921-2	9212-1
Analysis no.	12386	12387	12394	12395	12396	12862	12863	13744	(Wang et al., 1996)	
Locality	Shacun	Shacun	Shacun	Shacun	Shacun	Zhujiapu	Zhujiapu	Jiaoziyan	Raobazhai	Raobazhai
Rock type	Gabbro	Diorite	Gabbro	Q. diorite	Diorite	Px'enite	Gabbro	Gabbro	Gabbro	Px'enite
SiO_2	47.38	60.41	48.07	62.19	54.15	47.20	50.72	50.10	47.55	46.78
Al_2O_3	10.84	15.35	6.95	15.65	9.76	3.26	20.36	17.30	14.03	3.25
Fe_2O_3	11.01	6.25	11.88	5.57	8.80	12.08	8.71	8.52	10.80	10.37
MnO	0.17	0.10	0.19	0.09	0.14	0.21	0.07	0.14	0.20	0.16
MgO	11.08	3.36	15.94	2.37	11.97	22.71	2.96	6.47	9.50	18.24
CaO	13.57	4.96	11.54	4.51	7.18	12.39	6.44	9.65	9.63	17.52
Na_2O	1.84	3.58	1.20	3.67	2.08	0.36	5.23	3.20	2.74	0.25
K_2O	0.93	3.20	0.94	3.33	1.52	0.17	1.75	1.23	1.48	0.02
TiO_2	1.46	0.80	0.78	0.72	0.94	0.34	1.07	1.12	0.71	0.92
P_2O_5	0.18	0.33	0.13	0.26	0.30	0.04	0.79	0.29	0.24	0.01
LOI	0.97	0.78	1.75	0.66	2.16	0.46	0.93	0.45	3.37	2.41
Total	99.43	99.12	99.37	99.02	99.00	99.22	99.03	98.47	100.25	99.93
mg	69	54	75	48	75	81	43	63	66	79
Trace elements (ppm), by XRF										
Nb	4.8	10.8	3.5	10.2	8.5	1	9	7.68	2	0.95
Zr	84	226	90	205	152	26	509	122	61	22
Y	32	24	20	23	20	11	28	18	22	5.6
Sr	518	671	295	658	452	87	1493	923	727	224
Rb	20	77	27	91	40	3	52	23	31	1.2
Co	44	17	72	15	55	90	26		43	84
V	317	132	199	113	122	146	129		55	286
Ni	87	27	271	12	369	399	8		102	449
Cr	586	110	636	29	969	1224	6		345	1470
Ba	448	1514	492	1415	855	77	2370	636	1100	149
Ga	14	19	10	19	14	5	25			
Cu	39	31	85	16	23	87	139			
Zn	78	69	86	62	94	77	75			
Th	2	10	3	10	7	1	2	0.8	0.69	0.06
Pb	9	15	8	20	15	<1	10	6.59		
By ID (ppm)										
La	16.15	48.35	16.06	43.37	37.33	3.91	61.10	26.74	17.90	1.12
Ce	38.50	94.01	37.28	85.96	76.33	10.56	123.31	56.23	41.40	5.14
Nd	26.53	38.82	19.75	35.16	34.98	8.13	55.54	27.05	22.30	5.32
Sm	6.63	6.66	4.53	6.15	6.49	2.20	9.27	5.59	4.84	1.70
Eu	1.951	1.747	1.271	1.572	1.675	0.644	2.586	2.012	1.89	0.73
Gd	6.69	5.26	4.24	4.92	4.93	2.33	6.95	5.662	5.42	1.99
Tb								0.701	0.91	0.33
Dy	5.42	3.96	3.32	3.62	3.58	2.00	4.72	3.829		
Ho								0.701	1.17	0.37
Er	2.88	2.18	1.64	1.98	1.79	1.07	2.29	1.816		
Tm									0.45	0.12
Yb	2.26	1.98	1.35	1.80	1.41	0.93	1.88	1.51	2.64	0.63
Lu	0.331	0.307	0.194	0.278	0.213	0.136	0.277	0.224	0.34	0.08
$(La/Yb)_n$	4.7	16.1	7.9	16.0	17.5	2.8	21.5	11.7	4.5	1.2
Sm/Nd	0.250	0.172	0.229	0.175	0.186	0.271	0.167	0.207	0.217	0.320
Ba/Nb	93	140	141	139	101	77	263	83	550	157
La/Nb	3.4	4.5	4.6	4.3	4.4	3.9	6.8	3.5	9.0	1.2

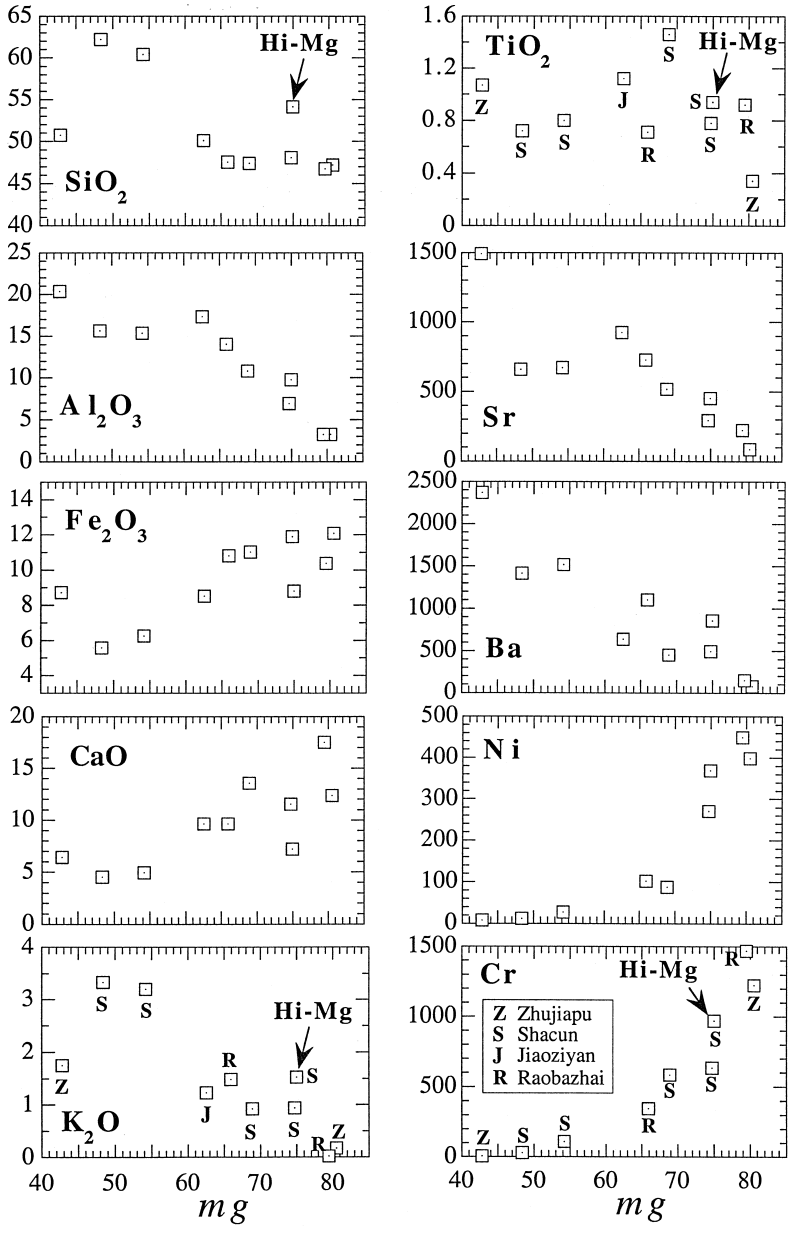

Fig. 2. Geochemical variation diagrams for major and trace elements as a function of mg values (as a rough index of differentiation). mg value is the molecular proportion of MgO/(MgO + FeO), assuming 90% of total iron as ferrous iron. Note that two rocks from Raobazhai fall outside of the trends in most cases. R = Raobazhai, Z = Zhujiapu, S = Shacun, J = Jiaoziyan.

sphene, thus, leading to low mg value, low Ni and Cr, but high Al, Ti, Sr and Ba contents.

(4) In the primitive mantle (PM) normalized geochemical spidergrams (Fig. 4) all the rocks show very distinctive negative anomalies in Nb, P and Ti, and positive anomalies in Pb. Negative Nb anomaly is most characteristic of subduction zone volcanic rocks or typical continental crust. Since a subduction

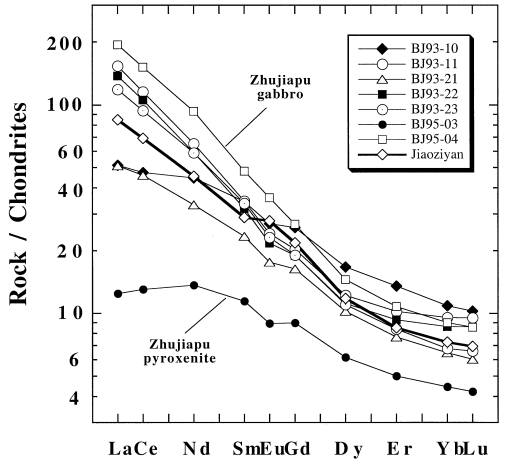

Fig. 3. Chondrite-normalized REE patterns for mafic–ultramafic rocks of the NDC. All gabbros and diorites are highly enriched in light REE's. The Zhujiapu pyroxenite pattern is consistent with that formed by accumulation of pyroxenes from a liquid of LREE-enriched pattern. Chondrite values [1.2× (Masuda et al., 1973); in ppm] used for normalisation are: La = 0.315, Ce = 0.813, Nd = 0.595, Sm = 0.193, Eu = 0.0722, Gd = 0.259, Dy = 0.325, Er = 0.213, Yb = 0.208, Lu = 0.0323.

is not considered plausible in the post-collisional tectonic setting in the Dabie terrane, the 'continental'

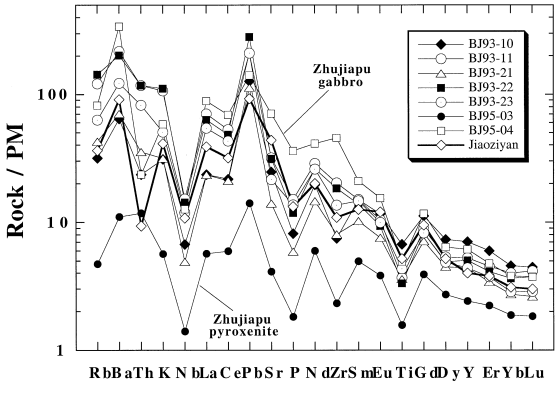

Fig. 4. PM normalized spidergrams of the mafic–ultramafic rocks. Conspicuous negative anomalies in Nb, P, and Ti and positive Pb anomalies are observed in all samples. The PM values (in ppm) used are from Sun and McDonough (1989): Rb = 0.635; Ba = 6.99; Th = 0.056; U = 0.021; K = 249; Nb = 0.713; La = 0.687; Ce = 1.775; Sr = 21.1; P = 96; Nd = 1.354; Zr = 11.2; Sm = 0.444; Eu = 0.168; Ti = 1300; Gd = 0.596; Dy = 0.737; Y = 4.55; Er = 0.48; Yb = 0.493; Lu = 0.077.

signature of mantle-derived magmas must have a special implication.

(5) La/Nb ratios in gabbros, diorites and pyroxenite are relatively uniform about 4 and so are Ba/Nb ratios about 100 (Fig. 5; Table 1). These values are substantially different from those of most intraplate volcanic rocks including N-MORB, OIB, alkali basalts and kimberlites which have La/Nb ratios of 2.5 to 0.5 and much smaller Ba/Nb ratios of 20 to 1 (Fig. 5). The data suggest a role of continental rocks (granitoids, granulites, sediments, etc.) in the magma genesis of the mafic–ultramafic suite.

In summary, the geochemical characteristics of these mantle-derived magmas and their differentiates are highly unusual in that they contain a clear continental signature which is unrelated to subduction

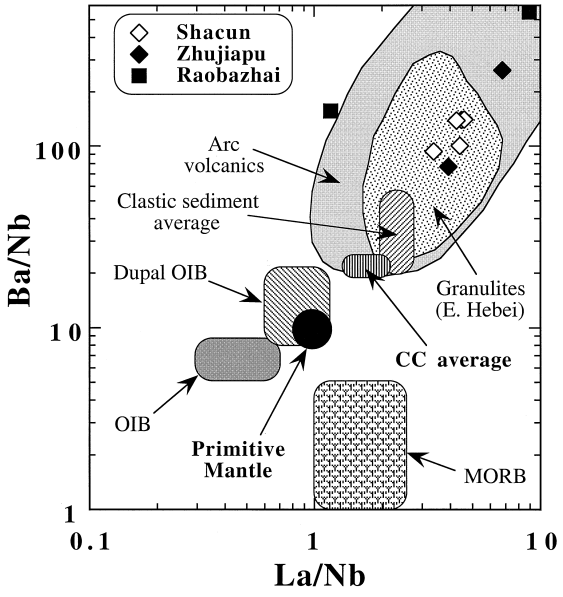

Fig. 5. Ba/Nb vs. La/Nb plot showing that the mafic–ultramafic rocks are characterized by high Ba/Nb and La/Nb ratios, falling in the fields of arc volcanics and Archean granulites from eastern Hebei (data from Jahn and Zhang, 1984). Magmatic differentiation tends to increase both ratios. The granulite data are used to infer the composition of the middle to lower continental crust, but not to imply a connection with the Sino-Korean craton. Data sources for other fields: PM (Sun and McDonough, 1989), CC (continental crust) average (Taylor and McLennan, 1985; Condie, 1993), Clastic sediment average (Condie, 1993), MORB, OIB and Dupal OIB (Le Roux, 1986).

Table 2
Whole-rock Rb–Sr and Sm–Nd isotopic compositions of mafic–ultramafic rocks from the NDC

Sample no.	Analysis no.	Rock type	Locality	[Rb] (ppm)	[Sr] (ppm)	$^{87}Rb/^{86}Sr$	$^{87}Sr/^{86}Sr$	$\pm 2\sigma_m$	I_{Sr} (120 Ma)
(A) North Dabie complex									
BJ93-10	12386	gabbro	Siling	19.7	515.5	0.111	0.707640	8	0.70745
BJ93-11	12387	diorite	Shacun	79.1	675.3	0.339	0.708141	7	0.70756
BJ93-21	12394	gabbro	Shacun	24.5	278.0	0.255	0.707885	7	0.70745
BJ93-22	12395	diorite (light)	Shacun	85.8	662.4	0.375	0.708556	7	0.70792
BJ93-23	12396	diorite (dark)	Shacun	39.1	429.7	0.263	0.708121	7	0.70767
BJ95-03	12862	pyroxenite	Zhujiapu	3.02	84.1	0.104	0.707689	6	0.70751
		(duplicate)		3.22	85.9	0.108	0.707709	5	0.70752
BJ95-04	12863	gabbro	Zhujiapu	51.3	1559	0.095	0.708171	6	0.70801
95DP-13P	13744	gabbro	Jiaoziyan	23.0	923.3	0.072	0.706839	6	0.70672
		(duplicate)					0.706862	6	
DZh-1a		diorite	Zhujiapu						
DZh-1b		diorite	Zhujiapu						
(B) Noth Huaiyang Flysch Belt									
9101		diorite	Shanqilihe	96.9	1147	0.245	0.709180	10	0.70876
9105		gabbro	Wangjiachong	38.9	731.3	0.154	0.709700	20	0.70944
9108		gabbro	Wangjiachong	6.17	1182	0.015	0.706790	20	0.70676

(1) $^{143}Nd/^{144}Nd$ ratios have been corrected for mass fractionation relative to $^{146}Nd/^{144}Nd = 0.7219$ and are reported relative to the La Jolla Nd standard = 0.511860 or Ames Nd standard = 0.511962.
(2) $^{87}Sr/^{86}Sr$ ratios have been corrected for mass fractionation relative to $^{86}Sr/^{88}Sr = 0.1194$ and are reported relative to the NBS-987 Sr standard = 0.710250.
(3) CHUR (chondritic uniform reservoir): $^{147}Sm/^{144}Nd = 0.1967$; $^{143}Nd/^{144}Nd = 0.512638$.
(4) Used in model age calculation, DM (depleted mantle): $^{147}Sm/^{144}Nd = 0.2137$; $^{143}Nd/^{144}Nd = 0.51315$.
(5) Blanks: Rb = 30 pg, Sr = 100 pg, Sm = 37 pg, Nd = 100 pg.

because this process was absent during the Cretaceous. It remains to be determined whether it means (1) crustal contamination during magma differentiation, (2) partial melting of mantle peridotites highly metasomatized by interaction with deeply subducted continental crust during the Triassic collision, or (3) a combination of both processes.

4.2. Mineral ages

4.2.1. Rb–Sr isotope systematics

Because the mafic and ultramafic rocks are not metamorphosed, we opted to use mineral isochron methods for dating the intrusive or cooling events. The results of isotopic analyses for whole-rock samples and constituent minerals are given in Tables 2 and 3, respectively. In Table 2, we include published data of three Cretaceous bodies (two gabbros and a diorite) emplaced in the North Huaiyang Belt. These rocks are isotopically identical to those of the present study, thus a similar petrogenesis is implied. A gabbro from Shacun (BJ93-21) yielded a Rb–Sr isochron age of 123 ± 6 (2σ) Ma (ISOPLOT, Model 3 solution), with $I_{Sr} = 0.70738 \pm 1$ (Fig. 6a). The isochron age is evidently controlled by biotite, so it is considered as a biotite cooling age. Fine-grained gabbroic dike (BJ95-04) from Zhujiapu gave a biotite–WR–plagioclase Rb–Sr isochron age of 118 ± 2 Ma, with $I_{Sr} = 0.70801 \pm 1$. Again, this is a biotite cooling age for the dike intrusion. The age of the coarse-grained intruded pyroxenite (BJ95-03) was not obtained by the Rb–Sr analyses due to slight open system behavior of the analyzed phases. However, the pyroxenite possesses an initial $^{87}Sr/^{86}Sr$ ratio of about 0.7075, distinctly lower than the 'geochemically' cogenetic gabbroic dike (Fig. 6b). This may suggest that crustal contamination has exerted variable effects on the two

[Sm] (ppm)	[Nd] (ppm)	$^{147}Sm/^{144}Nd$	$^{143}Nd/^{144}Nd$	$\pm 2\sigma_m$	$\varepsilon_{Nd}(0)$	$\varepsilon_{Nd}(T)$ (120 Ma)	f Sm/Nd	T_{DM} (Ga)	Reference
6.67	26.85	0.1503	0.511682	5	−18.6	−17.9	−0.24	3.50	This study
8.49	49.65	0.1034	0.511588	5	−20.5	−19.1	−0.47	2.15	This study
4.61	20.37	0.1368	0.511809	6	−16.2	−15.3	−0.30	2.64	This study
6.14	35.16	0.1056	0.511618	8	−19.9	−18.5	−0.46	2.15	This study
6.62	35.85	0.1116	0.511624	6	−19.8	−18.5	−0.43	2.27	This study
2.19	8.01	0.1650	0.511786	6	−16.6	−16.1	−0.16	4.22	This study
2.24	8.24	0.1644	0.511796	6	−16.4	−15.9	−0.16	4.14	This study
9.52	57.05	0.1009	0.511781	6	−16.7	−15.3	−0.49	1.84	This study
5.59	27.05	0.1249	0.512066	4	−11.2	−10.1	−0.37	1.86	This study
5.84	28.06	0.1258	0.512072	6	−11.0	−10.0	−0.36	1.86	This study
7.85	31.37	0.1512	0.511757	19	−17.2	−16.5	−0.23	3.37	Li et al. (1989a,b)
4.98	22.78	0.1322	0.511710	19	−18.1	−17.1	−0.33	2.68	Li et al. (1989a,b)
9.76	58.41	0.1010	0.511695	6	−18.4	−16.9	−0.49	1.96	Zhou et al. (1995a)
6.56	41.16	0.0964	0.511706	10	−18.2	−16.6	−0.51	1.87	Zhou et al. (1995a)
7.53	36.41	0.1250	0.512074	6	−11.0	−9.9	−0.36	1.84	Zhou et al. (1995a)

rocks, or they were derived from different sources, so their apparent cogenetic relationship was not significant. Overall, the whole-rock data points are seen scattered in the isochron diagram (Fig. 6b), but all of them have a rather small range of initial $^{87}Sr/^{86}Sr$ ratios from 0.7074 to 0.7080 (Table 2).

4.2.2. Sm–Nd mineral isochrons

Fig. 7 shows the Sm–Nd data points for WR and mineral separates. Like in the Rb–Sr systems, the WR data are scattered and no isochron relationship is discernible. However, mineral analyses of pyroxenite (BJ95-03) yielded an isochron age of 127 ± 70 (2σ) Ma, with $\varepsilon_{Nd}(T) = -16.1 \pm 0.5$. The large uncertainty is due to the very small range of $^{143}Nd/^{144}Nd$ ratios, even though they are well aligned and have a very small MSWD (0.02). Our data appear to be in conflict with a Sm–Nd mineral isochron age of 230 ± 44 Ma reported by Li et al. (1989a), who interpreted their age to represent a 'syncollisional' magmatic event induced by subduction of the continental crust. We shall discuss this point later.

4.2.3. Jiaoziyan Gabbro

The Jiaoziyan Gabbro is the largest Cretaceous mafic intrusion ($\approx 10 \times 3$ km) in the NDC (Fig. 1). A gabbronorite sample (95-DB-13P) was collected from an inner part of the intrusion and far away from the contact with the large Zhubuyuan granitic pluton. The sample is massive and medium-grained, and is composed of 40–45 modal % plagioclase, 30–35% augite, 10–15% orthopyroxene, about 5% biotite, and minor ilmenite, magnetite, and trace apatite. Petrographic description is given in Appendix A.

This sample was subjected to a detailed isotopic study mainly because a surprisingly 'old' Sm–Nd mineral isochron age of 238 ± 28 Ma (or 240 ± 48 Ma, recalculated using ISOPLOT with the same input errors as for the present work) was recently reported by Chen et al. (1997). Like Li et al. (1989a),

Table 3
Mineral Sr–Nd isotopic data of the gabbro–diorite–pyroxenite suite from the NDC

Sample no.	Rock type	Phase	Locality	[Rb] (ppm)	[Sr] (ppm)	$^{87}Rb/^{86}Sr$	$^{87}Sr/^{86}Sr$	$\pm 2\sigma_m$	I_{Sr} (120 Ma)
BJ93-10	gabbro	WR	Siling	19.71	515.53	0.111	0.707640	8	0.70745
		Cpx		3.77	75.56	0.144	0.707704	7	0.70746
		Hb		3.90	426.59	0.026	0.707429	7	0.70738
		Plag		75.40	1663.2	0.131	0.707800	6	0.70758
		Pl (dupl.)		67.18	1675.1	0.116	0.707746	8	0.70755
BJ93-21	gabbro	WR	Shacun	24.54	278.0	0.255	0.707885	7	0.70745
		Bi		194.7	111.1	5.077	0.716285	10	0.70763
		Cpx		2.30	82.59	0.0806	0.707504	8	0.70737
		Plag		9.30	1596.5	0.0169	0.707389	6	0.70736
BJ93-22	diorite	WR	Shacun	85.83	662.44	0.375	0.708556	7	0.70792
		Bi							
		Plag							
BJ93-23	diorite	WR	Shacun	39.09	429.69	0.263	0.708121	7	0.70767
		Hb		9.61	75.45	0.369	0.708241	8	0.70761
		Plag							
BJ95-03	pyroxenite	WR	Zhujiapu	3.02	84.11	0.1037	0.707689	6	0.70751
		Cpx		1.79	100.86	0.051	0.707691	8	0.70760
		Hb		5.60	260.88	0.062	0.707650	7	0.70754
		Plag		3.20	543.55	0.017	0.707837	7	0.70781
BJ95-04	gabbro	WR	Zhujiapu	51.32	1559.1	0.0953	0.708171	6	0.70801
		Bi		265.19	62.92	12.219	0.728461	9	0.70762
		Plag		8.20	2160.4	0.011	0.708025	7	0.70801
95DP-13P	gabbro	WR	Jiaoziyan	22.97	923.28	0.072	0.706839	6	0.70672
		(duplicate)					0.706862	6	
		Cpx		2.58	64.52	0.116	0.707099	7	0.70690
		(duplicate)							
		Opx		1.98	10.2	0.56	0.707980	6	0.70702
		(duplicate)							
		Plag		4.56	1668.7	0.0079	0.706804	5	0.70679
		(duplicate)							
		Bio		255.02	29.51	25.097	0.746304	6	0.70350
		(duplicate)							

(1) $^{143}Nd/^{144}Nd$ ratios was corrected for mass fractionation relative to $^{146}Nd/^{144}Nd = 0.7219$ and are reported relative to the La Jolla Nd standard = 0.511860 or Ames Nd standard = 0.511962.
(2) $^{87}Sr/^{86}Sr$ ratios have been corrected for mass fractionation relative to $^{86}Sr/^{88}Sr = 0.1194$ and are reported relative to the NBS-987 Sr standard = 0.710250.
(3) CHUR (chondritic uniform reservoir): $^{147}Sm/^{144}Nd = 0.1967$; $^{143}Nd/^{144}Nd = 0.512638$.
(4) Used in model age calculation, DM (depleted mantle): $^{147}Sm/^{144}Nd = 0.2137$; $^{143}Nd/^{144}Nd = 0.51315$.
(5) Blanks: Rb = 30 pg, Sr = 100 pg, Sm = 37 pg, Nd = 100 pg; 45 pg.

they interpreted this age as the time of syn-collisional intrusion and all Rb–Sr ages as the result of isotopic resetting by the strong Cretaceous thermal event when voluminous granitic plutons were intruded.

Our Rb–Sr analyses gave a five-point internal isochron age of 111 ± 4 Ma with $I_{Sr} = 0.7079 \pm 3$ (Fig. 8a). This is interpreted as the time when the gabbro cooled below the blocking temperature of biotite (≈ 300°C). A rough estimate of cooling rate for such a small gabbroic pluton, assuming reasonable magma density (3000 kg/m^3), thermal expansion (5×10^{-5}/deg), diffusivity (10^{-6} m^2/s), viscosity (10^3 Pa/s), pluton dimension (1.5 km from center), and temperature difference between magma and the surrounding ($\Delta T = 500$°C), suggests that the pluton, with convective heat dissipation, could cool down to 300°C within 1 Ma. In other words, the

[Sm] (ppm)	[Nd] (ppm)	$^{147}Sm/^{144}Nd$	$^{143}Nd/^{144}Nd$	$\pm 2\sigma_m$	$\varepsilon_{Nd}(0)$	$\varepsilon_{Nd}(T)$ (120 Ma)	f Sm/Nd	T_{DM} (Ma)
6.67	26.85	0.1503	0.511682	5	−18.6	−17.9	−0.24	3500
4.61	20.37	0.1368	0.511809	6	−16.2	−15.3	−0.30	2643
6.14	35.16	0.1056	0.511618	8	−19.9	−18.5	−0.46	2152
6.62	35.85	0.1116	0.511624	6	−19.8	−18.5	−0.43	2268
2.19	8.01	0.1650	0.511786	6	−16.6	−16.1	−0.16	4224
2.95	10.47	0.1701	0.511790	6	−16.5	−16.1	−0.14	4697
6.29	24.71	0.1540	0.511780	6	−16.7	−16.1	−0.22	3469
4.12	24.63	0.1010	0.511733	6	−17.7	−16.2	−0.49	1911
9.52	57.05	0.1009	0.511781	6	−16.7	−15.3	−0.49	1845
5.59	27.05	0.1249	0.512066	4	−11.2	−10.1	−0.37	1855
5.839	28.057	0.1258	0.512072	6	−11.0	−10.0	−0.36	1864
14.45	55.26	0.1581	0.512081	4	−10.9	−10.3	−0.20	2912
14.481	53.934	0.1623	0.512075	5	−11.0	−10.5	−0.17	3165
0.92	3.61	0.1541	0.512040	18	−11.7	−11.0	−0.22	2822
0.938	3.766	0.1506	0.512050	6	−11.5	−10.8	−0.23	2643
0.85	7.22	0.0715	0.511991	6	−12.6	−10.7	−0.64	1241
0.886	7.668	0.0698	0.511979	5	−12.9	−10.9	−0.65	1239
0.29	1.82	0.0966	0.512043	9	−11.6	−10.1	−0.51	1439
0.586	3.547	0.0999	0.512040	5	−11.7	−10.2	−0.49	1484

intrusive ages of Jiaoziyan and the smaller gabbroic and dioritic bodies would be at most a few Ma older than the biotite ages.

The inset of Fig. 8a shows that individual phases were not in isotopic equilibrium at the time of 110–120 Ma. A visual estimate of the 'initial ratios' at 111 Ma indicates that I_{Sr} values (= intercepts of the lines parallel to the biotite isochron) increase in the order from WR–Plag–Bio–Cpx–Opx. As shown in Table 3, the calculated I_{Sr} (120 Ma) vary from 0.70672 to 0.70702, except for the biotite whose I_{Sr} is extremely sensitive to age correction due to its very high Rb/Sr ratio (≈ 25). The difference of 0.00030 is 50 times of the analytical precision, or 15 times of the 'accuracy' derived from our long-term duplicate analyses of isotope standards, hence it is considered significant, indicating isotope non-equilibrium. The fact that the WR data point does not fall

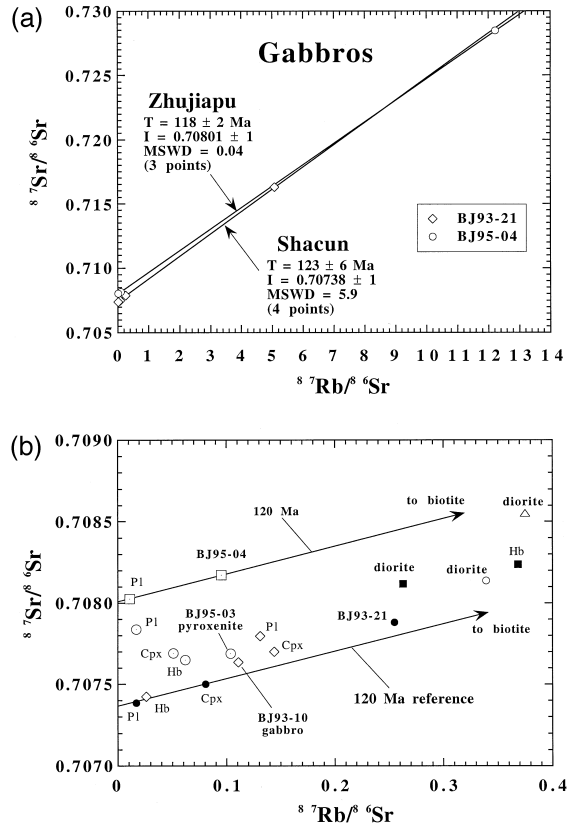

Fig. 6. (a) Rb–Sr mineral isochrons for gabbros from Shacun (BJ95-21) and Zhujiapu (BJ95-04), (b) WR (whole-rock) and mineral Rb–Sr data for other samples. Each set of symbols represents WR and minerals from the same sample. Note that the WR data are highly scattered, indicating heterogeneity of their initial ratios. The mineral data for BJ93-03 and BJ93-10 do not form isochrons, probably due to post-magmatic alteration.

within the polygon formed by the other 4 phases suggests that some other phase(s) not analyzed must be responsible for balancing the WR isotopic composition.

Sm–Nd isotope analyses also failed to produce any internal isochron (Fig. 8b). We are confident that the scatter was not due to analytical errors as each data point was confirmed by duplicate analysis. The slight shift between first and duplicate runs can be ascribed to some heterogeneity of the mineral compositions, because in our experiments only coarse mineral grains, without pulverization, were put directly into dissolution. Due to the variable contents of minute inclusions, different aliquots may have slightly different compositions. We note here once again that, as in the Rb–Sr system, the WR data point does not plot within the polygon of the four constituent phases. Evidently, some unanalyzed accessory minerals must be present to account for the isotope mass balance.

In any case, both the Rb–Sr and Sm–Nd data indicate that the constituent minerals of the Jiaoziyan Gabbro are not in isotopic equilibrium. To this point, we do not understand the isochron relationship reported by previous workers (e.g., Chen et al., 1997). Interpretation of this disequilibrated mineral assemblage is not easy. Concomittant crustal contamination during magmatic differentiation, similar to the AFC process (assimilation and fractional crystallisation) of Taylor (1980) and DePaolo (1981), may result in isotopic difference between the early and late precipitated phases if assimilation continues. The crystallisation of Cpx, Opx and Plag was probably near-contemporaneous, only biotite can be shown petrographically as a late phase. At 120 Ma, the sequence of increase in initial $^{143}Nd/^{144}Nd$ ratio (I_{Nd}) is from Plag ≈ Opx to Cpx to Bio (Fig. 8b); and this could be interpreted by a hypothesis of upper crustal contamination (higher I_{Nd}) in a liquid derived from a source dominated by lower crustal component (lower I_{Nd}) as we advocate below (Sec-

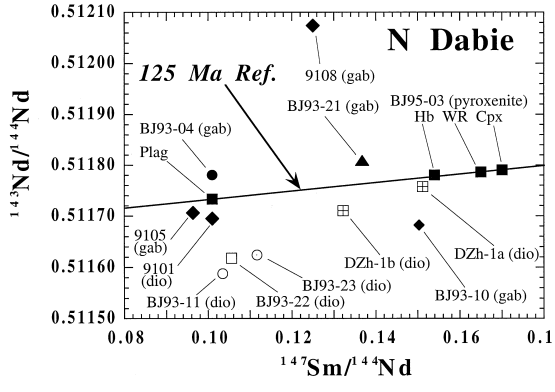

Fig. 7. Sm–Nd isochron diagram for the mafic–ultramafic rocks. WR data are highly scattered, indicating heterogeneity of their initial ratios. Mineral data of Zhujiapu pyroxenite (BJ93-03) fall on a 125 Ma reference isochron. The variation of isotope ratios is too small to obtain an age of satisfactory precision (calculated isochron age = 127 ± 70 Ma).

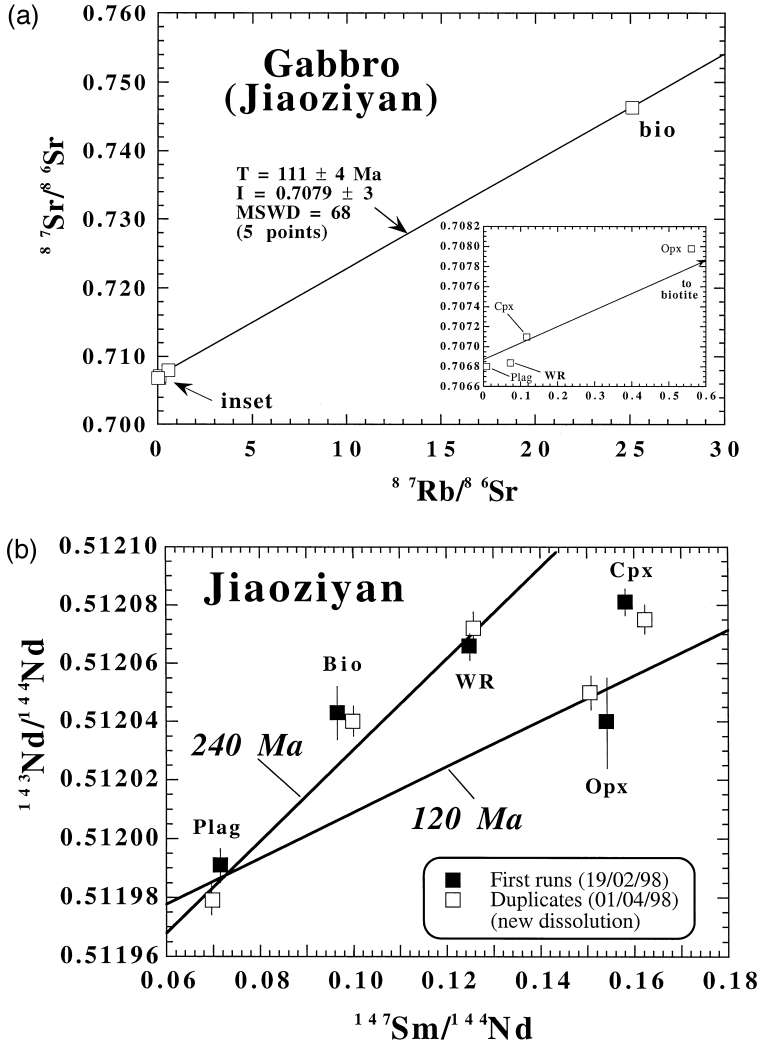

Fig. 8. (a) Rb–Sr isochron diagram for the Jiaoziyan gabbro. WR and constituent phases (Opx, Cpx, Plag) do not form a linear array with biotite, suggesting that these minerals were not in isotope equilibrium. (b) Sm–Nd isotopic data showing the absence of isochron relationship between WR and constituent minerals. The data scatter is confirmed by duplicate analyses.

tion 4.3). However, since the upper crust has a higher $^{87}Sr/^{86}Sr$ ratio, this does not explain the lower $^{87}Sr/^{86}Sr$ ratio observed in Plag (inset of Fig. 8a).

Alternatively, the Sr isotopic disequilibrium might be explained by post-magmatic alteration effect. Excluding the biotite data, whose I_{Sr} value strongly depends on the assigned age, the three phases (Cpx, Opx and Plag) appear to show their relative susceptibility toward crustal contamination as a function of their Sr concentrations. Indeed, the sequence of increasing I_{Sr} (Fig. 8a) is from Plag (Sr = 1670 ppm) to Cpx (65 ppm) to Opx (10 ppm).

We conclude that during the intrusion of the Jiaoziyan Gabbro an AFC process was probably in effect, causing the precipitated phases not in isotopic equilibrium with each other. Consequently, no mineral Sm–Nd isochron could have been established.

Alteration effect on Nd isotope composition is probably invisible on this little altered gabbro (see Appendix A for petrography), but it may be significant on the Sr isotope compositions.

4.2.4. Ar–Ar plateau ages

A whole-rock sample of anorthosite dike, a hornblende and a plagioclase from a gabbro of Zhujiapu massif were dated by the Ar–Ar method. The analytical data are presented in Table 4 and the age plateaux are displayed in Fig. 9. The anothositic dike has an age of 116 ± 3 Ma (Fig. 9a), which is identical to the plagioclase age of gabbro (118 ± 3 Ma; Fig. 9c). These two ages are indistinguishable from the biotite–WR–plagioclase Rb–Sr isochron age (118 ± 2 Ma), and are also consistent with the similar blocking temperatures (≈ 300°C) for plagioclase Ar–Ar and biotite Rb–Sr systems. Hornblende of the same gabbro sample gave 131 ± 3 Ma (Fig. 9b); this is explained by the higher blocking temperature of ≈ 500–550°C. We interpret the age as the time close to magmatic intrusion.

Hacker and Wang (1995) dated hornblendes by Ar–Ar from a diorite near Luzhen (about 20 km NW of Tongcheng) and a gabbro (about 20 km WNW of Tongcheng), both in the NE corner of the Dabie terrane. The diorite gave a plateau age of 134 ± 1 (2σ) Ma, whereas the gabbro yielded 130 ± 1 Ma.

4.2.5. Conclusion from the age studies

In addition to our age data outlined above, Hacker et al. (1998) reported two zircon ages of 129 ± 2 Ma (by SHRIMP) and 125 ± 2 Ma (by TIMS) for a gabbro from a locality near Mozitan. This is considered to be the best age determination for the gabbroic intrusions in the NDC. We therefore conclude from all the geochronological information that, regardless of their occurrences as dike, stock, or pluton, most of the gabbro, diorite and pyroxenite in the NDC as well as in the North Huaiyang Flysch Belt were emplaced in a short time span from 130 to 115 Ma. This period coincides with the massive intrusion of granitic rocks (Chen et al., 1991; Zhou et al., 1992; Chen et al., 1995). These mafic–ultramafic intrusive rocks seem to share the same Sr–Nd isotopic characteristics with the granites (to be discussed below). We relate these characteristics to the effect of the Triassic continental collision and subsequent crust–mantle interaction (mixing of sources).

4.3. Whole-rock Nd–Sr isotopic characteristics and genesis of highly negative ε_{Nd} mantle-derived basic magmas

The results of whole-rock Rb–Sr and Sm–Nd isotopic analyses, together with some published data

---

Notes to Table 4:

J-value: weighted mean of three fusions of irradiation standard LP-6 biotite, having a K–Ar age of 127.7 ± 1.4 Ma (Odin et al., 1982).

T (°C) = temperature with uncertainty of ± 2°C.

The date is obtained by using the following equations:

$$\text{Date} = \frac{1}{\lambda}\ln\left(1 + J\frac{^{40}\text{Ar}*}{^{39}\text{Ar}_{\text{K}}}\right),$$

and

$$\frac{^{40}\text{Ar}*}{^{39}\text{Ar}_{\text{K}}} = \frac{\left[^{40}\text{Ar}/^{39}\text{Ar}\right]_{\text{m}} - 295.5\left[^{36}\text{Ar}/^{39}\text{Ar}\right]_{\text{m}} + 295.5\left[^{36}\text{Ar}/^{37}\text{Ar}\right]_{\text{Ca}}\left[^{37}\text{Ar}/^{39}\text{Ar}\right]_{\text{m}}}{1 - \left[^{39}\text{Ar}/^{37}\text{Ar}\right]_{\text{Ca}}\left[^{37}\text{Ar}/^{39}\text{Ar}\right]_{\text{m}}} - \left[\frac{^{40}\text{Ar}}{^{39}\text{Ar}}\right]_{\text{K}}$$

where $[]_{\text{Ca}}$ and $[]_{\text{K}}$ = isotope ratios of argon extracted from irradiated calcium and potassium salts (values cited in the paper of Lo and Lee, 1994) and $[]_{\text{m}}$ = isotope ratio of argon extracted from irradiated unknown.

Date (Ma) = the date calculated using the following decay constants: $\lambda_{\varepsilon} = 0.581 \times 10^{-10}$ year^{-1}; $\lambda_{\beta} = 4.962 \times 10^{-10}$ year^{-1}; $\lambda = 5.543 \times 10^{-10}$ year^{-1}; $^{40}\text{K}/\text{K}$ 0.01167 at.%.

Uncertainty for $^{40}\text{Ar}*$ and $^{39}\text{Ar}_{\text{K}}$ volumes are $\pm 5\%$.

Cum. ^{39}Ar = cumulative fractions of $^{39}\text{Ar}_{\text{K}}$ and $^{40}\text{Ar}*$ released in each step.

The quoted error is one standard deviation and does not include the error in the *J*-value, the standard error, or the error in the interference corrections.

Integrated date = the date and error calculated from the sum total gas from all steps; the error includes the error in *J*-value.

Plateau date = the data and error calculated from the sum total gas from those steps, the ages of which fall within 2 S.D. of each other; the error includes the error in *J*-value.

on similar rocks from the North Huaiyang Belt, are given in Table 2. We underline the characteristic and very spectacular highly negative $\varepsilon_{Nd}(T)$ values for these mantle-derived rocks. Depleted mantle model ages (T_{DM}) for the mafic–ultramafic rocks range from 4.2 to 1.8 Ga (Table 2). T_{DM} values calculated from high Sm/Nd rocks ($^{147}Sm/^{144}Nd = 0.16$) often gave spurious and insignificant age information

Table 4
$^{40}Ar/^{39}Ar$ age data for anorthosite and gabbro samples of the NDC

T (°C) cum.	^{39}ArK	Atmos. (%)	$^{36}Ar/^{39}Ar$	$^{37}Ar/^{39}Ar$	$^{38}Ar/^{39}Ar$	$^{40}Ar/^{39}Ar$	$^{40}Ar/^{39}Ar$	Date (Ma)
DB49C whole rock, Anorthosite dyke, Zhujiapu, Dabie Mt.								
550	0.051	50.129	0.2061E + 00	0.8193E + 02	0.5168E − 01	0.1092E + 03	0.5298E + 03	147.2 ± 6.0
650	0.200	7.541	0.2287E − 01	0.3686E + 02	0.1776E − 01	0.5281E + 02	0.2309E + 04	128.7 ± 3.5
750	0.313	2.406	0.8486E − 02	0.1871E + 02	0.1531E − 01	0.4567E + 02	0.5381E + 04	116.5 ± 5.3
850	0.408	0.636	0.8433E − 02	0.2934E + 02	0.1471E − 01	0.4426E + 02	0.5249E + 04	115.8 ± 5.9
950	0.499	0.058	0.9534E − 02	0.3705E + 02	0.1709E − 01	0.4369E + 02	0.4583E + 04	115.5 ± 4.4
1000	0.554	5.062	0.1827E − 01	0.4067E + 02	0.1933E − 01	0.4613E + 02	0.2525E + 04	116.1 ± 6.6
1100	0.688	8.939	0.2067E − 01	0.2171E + 02	0.1889E − 01	0.5005E + 02	0.2422E + 04	119.2 ± 3.5
1200	1.000	14.429	0.2667E − 01	0.5123E + 01	0.1832E − 01	0.5198E + 02	0.1949E + 04	115.2 ± 2.9
Sample mass = 0.0800 g								
J-value = 0.0014789 ± 0.000037193								
Integrated date = 119.7 ± 3.1 Ma								
Plateau date = 116.2 ± 3.0 Ma (750–1200°C)								
DB49B hornblende, Gabbro, Zhujiapu, Dabie Mt.								
550	0.161	29.096	0.7528E − 01	0.8248E + 01	0.3118E − 01	0.7435E + 02	0.9876E + 03	136.1 ± 3.7
600	0.350	3.716	0.9664E − 02	0.1085E + 02	0.1711E − 01	0.5487E + 02	0.5678E + 04	136.6 ± 3.9
700	0.553	0.001	0.6875E − 02	0.3281E + 02	0.1691E − 01	0.5094E + 02	0.7409E + 04	133.7 ± 4.6
800	0.638	0.449	0.1384E − 01	0.5150E + 02	0.2274E − 01	0.4662E + 02	0.3368E + 04	123.7 ± 6.1
900	0.738	0.420	0.1559E − 01	0.5864E + 02	0.2008E − 01	0.4516E + 02	0.2896E + 04	120.6 ± 4.8
1000	0.796	2.237	0.2558E − 01	0.8610E + 02	0.2897E − 01	0.4791E + 02	0.1873E + 04	127.7 ± 7.6
1080	0.840	15.380	0.4550E − 01	0.6432E + 02	0.3673E − 01	0.5594E + 02	0.1229E + 04	127.2 ± 6.6
1160	0.935	19.414	0.4638E − 01	0.2840E + 02	0.3348E − 01	0.5960E + 02	0.1285E + 04	125.9 ± 4.5
1230	1.000	29.637	0.6236E − 01	0.4196E + 04	0.3843E − 01	0.6220E + 02	0.9975E + 03	113.1 ± 5.5
Sample mass = 0.1280 g								
J-value = 0.0014789 ± 0.000037193								
Integrated date = 129.8 ± 3.4 Ma								
Plateau date = 130.9 ± 3.4 Ma (550–1160°C)								
DB49B plagioclase, Gabbro, Zhujiapu, Dabie Mt.								
550	0.048	53.756	0.3134E + 00	0.2223E + 02	0.1116E + 00	0.1692E + 03	0.5399E + 03	200.2 ± 6.3
620	0.111	27.021	0.5465E − 01	0.1504E + 00	0.3510E − 01	0.5975E + 02	0.1093E + 04	112.7 ± 6.5
700	0.192	9.035	0.2796E − 01	0.4928E + 02	0.1264E − 01	0.5038E + 02	0.1802E + 04	122.0 ± 7.2
800	0.283	0.000	0.9945E − 02	0.5162E + 02	0.2087E − 01	0.4825E + 02	0.4852E + 04	128.5 ± 6.2
900	0.363	0.000	0.6844E − 02	0.6504E + 02	0.1380E − 01	0.4338E + 02	0.6339E + 04	116.9 ± 8.1
1000	0.451	0.000	0.9125E − 03	0.7105E + 01	0.7081E − 02	0.4330E + 02	0.4745E + 05	112.4 ± 5.8
1060	0.532	7.442	0.1563E − 01	0.1783E + 02	0.1993E − 01	0.4405E + 02	0.2818E + 04	106.8 ± 4.8
1120	0.665	4.627	0.1798E − 01	0.4131E + 02	0.2164E − 01	0.4761E + 02	0.2647E + 04	120.3 ± 4.4
1180	0.932	15.349	0.3225E − 01	0.1716E + 02	0.1998E − 01	0.5368E + 02	0.1665E + 04	118.8 ± 3.8
1240	1.000	6.298	0.2497E − 01	0.5793E + 02	0.3082E − 01	0.4790E + 02	0.1918E + 04	120.3 ± 5.6
Sample mass = 0.0552 g								
J-value = 0.0014789 ± 0.000037193								
Integrated date = 122.1 ± 3.3 Ma								
Plateau date = 118.0 ± 3.2 Ma								

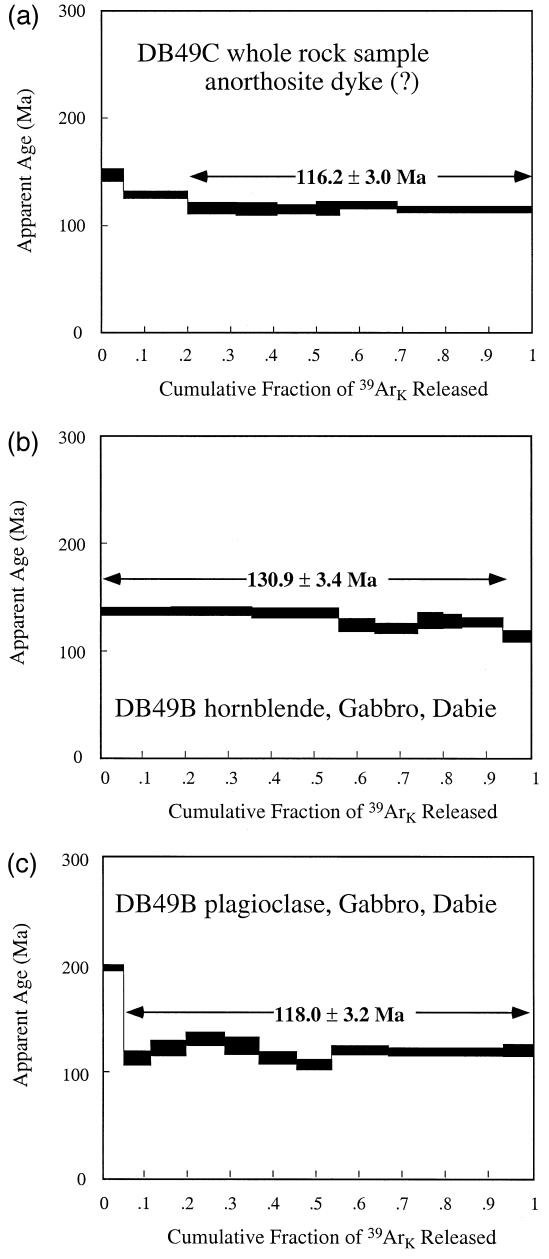

Fig. 9. ^{40}Ar–^{39}Ar plateau ages of (a) an anothosite WR, (b) a hornblende and (c) a plagioclase of gabbro from Zhujiapu.

with large uncertainties. If such rock (pyroxenite BJ95-03) is excluded, then the range of T_{DM} is reduced to 3.5–1.8 Ga, which, coincidentally, is identical to that of Cretaceous granitic intrusions as well as older granitic gneisses from the Dabie terrane (Chen and Jahn, 1998).

From an extensive compilation of Sm–Nd isotopic compositions and T_{DM} values for intrusive granitoids, sedimentary and metamorphic rocks, Chen and Jahn (1998) demonstrated that the Yangtze–Cathaysia craton is essentially made up of Proterozoic rocks, at least for the middle to upper crustal levels. The occurrence of an Archean granitic gneiss in the Kongling Group in Hubei Province (Zheng et al., 1991; Ames et al., 1996) is very unusual, and its tectonic significance is at best ambiguous. However, the presence of Archean model ages (= 2.5 Ga) in the Dabie terrane is something unusual and may be indicative of exposure of an ancient lower crust of the Yangtze craton whose age could be Archean, or of slices of Archean crust from the Sino-Korean craton that were mixed up in the exhumation of the Dabie UHP rocks. At any rate, the Dabie orogen appears to contain some Archean crustal protolith components.

In an $\varepsilon_{Nd}(T)$ vs. I_{Sr} diagram (Fig. 10a), the data of mafic and ultramafic intrusions from both NDC and North Huaiyang Belt lie in the enriched extension of the 'mantle array' defined by mantle-derived rocks. The Cretaceous granitoids of Dabieshan (Zhou et al., 1995b,c; Xie et al., 1996) occupy a field that overlaps the mafic–ultramafic rocks. They all are characterized by $\varepsilon_{Nd}(T)$ of −15 to −20 and I_{Sr} of 0.707 to 0.710. The data are distinguished from the UHP mafic–ultramafic rocks, such as those from Rizhao, Bixiling and Maowu (Fig. 10a). The geochemical argument presented earlier required a significant role of crustal contamination either in the mantle sources or during magma ascent and differentiation.

From the Nd–Sr isotopic consideration, the upper crust is not likely a good candidate as the major contaminant (Fig. 10a). In the apparent absence of very old upper crust in the Yangtze craton (Chen and Jahn, 1998), the best candidate for crustal contaminant is the subducted lower crust. We do not know exactly its isotopic characteristics, but a good guess from our compilation work (Chen and Jahn, 1998) would place it as marked 'Yangtze lower crust' in Fig. 10a. The single data point of Kongling gneiss is shown for comparison (data from Ames et al., 1996),

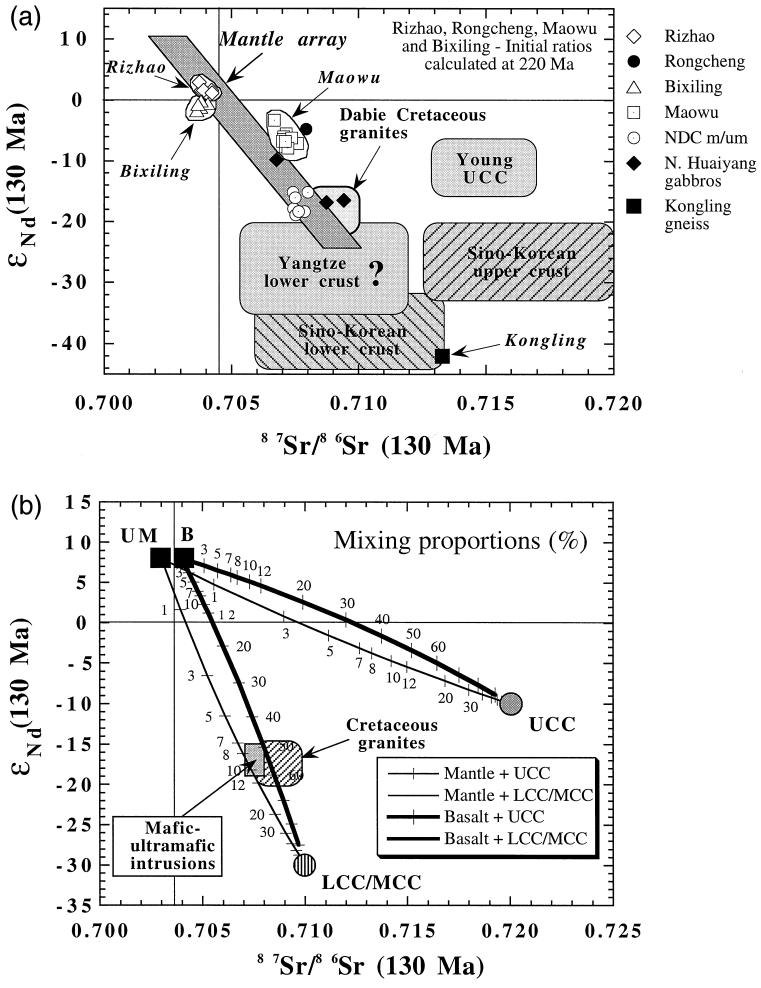

Fig. 10. (a) $\varepsilon_{Nd}(T)$ vs. initial $^{87}Sr/^{86}Sr$ plot for a variety of mafic–ultramafic rocks from the Dabie orogen. Those from Rizhao, Rongcheng, Maowu and Bixiling represent UHP assemblages formed at $\approx$ 220 Ma during the Triassic collision. Those from the NDC are characterized by the highly negative $\varepsilon_{Nd}(T)$ values (-15 to -20), identical to that of the Cretaceous granitic intrusions. Possible isotopic fields for different crustal segments are shown for comparison. Data sources: Rizhao, Rongcheng (Jahn, 1998), Bixiling (Chavagnac and Jahn, 1996), Maowu (Jahn et al., 1999b), Cretaceous granites (Zhou et al., 1995b,c; Xie et al., 1996; Chen and Jahn, 1998), N. Huaiyang gabbros (Zhou et al., 1995c), Kongling gneiss (Ames et al., 1996). Other fields (literature data). (b) Mixing calculations for source and melt contaminations. The mixing parameters used are:

	UM	Basalt	UCC	MCC-LCC
$^{87}Sr/^{86}Sr$	0.703	0.704	0.720	0.710
[Sr] ppm	20	150	350	300
ε_{Nd}	+8	+8	−10	−30
[Sm] ppm	0.42	3.5	5.2	4.8
[Nd] ppm	1.2	15	26	24
Sr/Nd	16.7	10	13.5	12.5

UM denotes upper mantle peridotites, UCC, upper continental crust (elemental data from Taylor and McLennan (1985)), MCC-LCC, middle to lower crust (data of middle crust from Rudnick and Fountain (1995)).

but we do not think that it is representative of the Yangtze craton due to its singularity. In addition, available Pb isotope data for the Cretaceous granitic intrusions in Dabieshan (Zhang et al., 1995) indicate

their intraplate affinity and unradiogenic middle-lower crustal origin.

Highly negative $\varepsilon_{Nd}(T)$ values for mantle-derived mafic–ultramafic rocks have also been found in the late Proterozoic ($\approx$ 670 Ma) Dovyren layered intrusion in northern Baikal region, Russia (Amelin et al., 1996). Gabbro, troctolite, gabbronorite, dunite, plagioclase peridotite, and diabasic sill are the lithological varieties, and they all have $\varepsilon_{Nd}(T)$ values of about -14 to -15 and I_{Sr} from 0.710 to 0.714. Using geochemical and isotopic (Nd–Sr–Pb) arguments, Amelin et al. (1996) concluded that the rocks were most likely produced by partial melting of depleted lherzolite which was contaminated by subducted sediments (or continental crust) prior to the melting event.

For the present case, we believe that crustal contamination in the mantle source is also the most probable interpretation for the isotopic and geochemical features. A simple modeling for source contamination (Fig. 10b) indicates that mixing the upper mantle peridotite with about 10% of subducted continental mass with middle to lower crustal characteristics would suffice to explain the present Sr–Nd isotopic features of the mafic–ultramafic intrusions. Injection of 10% of crustal materials into the mantle would not change much the major element composition, but it could significantly increase trace element abundances of the mantle peridotites. In so far as the higher Sr isotopic ratios of the Cretaceous granites are concerned (Fig. 10a), it appears that their sources might have involved some upper crustal materials.

Crustal contamination during magma ascent might have occurred, but it cannot explain the observed isotopic and geochemical features from the mass balance consideration. The isotopic constraint favors the middle to lower but not the upper crustal contamination. The composition and lithological nature of the lower crust has long been debated. It is composed of rocks in the granulite facies and is lithologically heterogeneous (Rudnick and Fountain, 1995). If it is of normal mafic or basaltic composition, it is unlikely to have developed a highly negative ε_{Nd} composition as required. If it is of intermediate composition and characterised by light rare earth enrichment, it must be old, likely to be of early Proterozoic or Archean age. It is such composition that is used in the present calculation (see Fig. 10b for parameters). Fig. 10b shows two mixing curves of a basaltic magma subjected to an upper and a middle-lower crustal contamination. However, in order to change the Nd isotopic composition of a mantle-derived liquid from an ε_{Nd} of $+8$ (assumption) to -15 to -20, it requires an assimilation of 50–60% of mid-lower crustal rocks. Let alone the problem of heat budget, such a voluminous assimilation would severely modified the major element composition of the magmas. For example, the SiO_2 contents would have to be significantly increased, but this is not the case for the gabbros and pyroxenites in question (Table 1). Note that the Sr–Nd concentrations of basalt used in the calculation are much lower than those of the gabbros, which, in our model interpretation, are derived from a metasomatised mantle. On the other hand, as constrained by SiO_2 contents, a few percent of crustal contamination in gabbroic magmas would not suffice to explain the very large negative Nb anomalies in the spidergrams (Fig. 4) or the high La/Nb and Ba/Nb ratios as shown in Fig. 5.

We therefore conclude that the present unusual isotopic compositions of the mafic–ultramafic intrusions are a result of source mixing and provide strong evidence for crust–mantle interaction when a segment of continental crust was deeply subducted and some of it remained at mantle depth after exhumation of UHP metamorphic rocks during the post-collisional extensional phase.

4.4. Tectonic implications

Hacker et al. (1996) reviewed the existing tectonic models for the Dabie UHP terrane. The general agreement for all models includes: (1) the Yangtze and Sino-Korean cratons are the principal continental colliders, only some models speculatively include intervening micro-continents or intraoceanic arcs, and (2) a northward subduction of the Yangtze craton, because the fold-thrust belt in the southern part of the orogen verges southward, and metamorphic pressures increase northward from blueschist to coesite-bearing eclogite. By contrast, the disagreement abounds, particularly concerning the NDC. This unit has been regarded as (1) a less deeply subducted part of the Yangtze craton (Okay and Sengör, 1992), (2)

a metamorphosed ophiolite melange complex (Xu et al., 1992, 1994), (3) a Paleozoic arc complex (Zhai et al., 1994; Wang et al., 1996), (4) part of the Sino-Korean craton in the hanging wall of the subduction zone (Liou et al., 1996; Zhang et al., 1996), or (5) extruded subduction assemblage, which involved a micro-continent of transition crust and the Yangtze basement, onto the Sino-Korean craton following an Alpine indentation model (Hacker et al., 1996), or most recently, (6) a Cretaceous magmatic complex formed in the post-collisional extension (Hacker et al., 1998).

Geochemical and isotopic constraints to the tectonic evolution of the entire Dabie orogen may be summarized below: (1) the subducted continental crust is dominantly of Proterozoic ages, probably with the Yangtze affinity (Chen and Jahn, 1998; Hacker et al., 1998; Jahn, 1998), (2) the Nd isotopic compositions of UHP eclogites suggest that the subducted crust was a mature, ancient and cold crust, not of transition crustal nature (Jahn et al., 1995; Jahn, 1998), (3) none of the mafic–ultramafic rocks in both central Dabie UHP and northern Dabie gneiss terranes can be identified as ophiolite suites (Jahn, 1998; this paper), (4) Archean isotope signature is rarely found in any Dabie lithologic units (Chen and Jahn, 1998), but this does not exclude a minor role of Sino-Korean craton, traditionally considered as of Archean age, in the making of the collisional orogen, (5) if the sediments of the North Huaiyang Flysch Belt (= Foziling Group) are considered as an accretionary wedge derived from the Sino-Korean craton in Devonian (Mattauer et al., 1985), then the hangingwall hypothesis is not at variance with the presently known age and isotopic data which yield Sm–Nd T_{DM} ages of 1.6 to 2.2 Ga (Li et al., 1994; Chen and Jahn, 1998; Jahn et al., 1999b).

The geochemical and isotopic analyses of mafic and ultramafic intrusions of the NDC suggest a strong interaction between mantle and subducted continental crustal rocks. The process is considered to have occurred in the post-collisional epoch, and between the hot asthenosphere and 'trapped' lower continental crust after most subducted continental slices were uplifted. The tectonic scenario can be illustrated by a model shown in Fig. 11.

Fig. 11a describes the early stage of collision at about 230 Ma between the Yangtze and Sino-Korean cratons. Subduction of the continental lithosphere ceased when it reached 100–120 km of depth due mainly to its buoyancy. However, the denser oceanic lithosphere, of which the oceanic crust has dehydrated and converted to eclogite, continued to subduct and eventually detached from the continental lithosphere (e.g., Davis and von Blanckenburg, 1995). Once the detachment took place, the continental lithosphere, particularly the sialic crustal component, would have rebounded, uplifted or vertically extruded rapidly (Fig. 11b), as hypothesized by Hacker et al. (1996). By then UHP assemblages would have recorded their exhumation time at about 210–220 Ma (Ames et al., 1993; Li et al., 1993; Hacker and Wang, 1995; Ames et al., 1996; Chavagnac and Jahn, 1996; Rowley et al., 1997; Hacker et al., 1998).

Field data indicate that, unlike the case of the Hercynian belt in western Europe, only limited volumes of syntectonic granites were formed during the collision and subsequent exhumation of UHP rocks. This is the most remarkable aspect of the Dabie orogen. It appears that the absence or limited amount of syn-collisional granites and the widespread preservation of UHP metamorphic assemblages are mainly due to the low water activity as well as the rapid rate of initial exhumation (see also Liou et al., 1997). The first post-tectonic granitic intrusion took place long (almost 100 Ma) after the initial collision event. Moreover, the available Sr–Nd–Pb isotopic compositions of the Cretaceous granites (mainly of alkaline variety) indicate their intraplate affinity and unradiogenic lower crustal origin (Zhang et al., 1995; Zhou et al., 1995b,c; Xie et al., 1996).

Fig. 11c illustrates the scenario when massive granitic magmas and volumetrically much smaller but numerous basic and ultrabasic stocks, plutons or dikes were emplaced in an extensional phase at about 130–120 Ma. Heat source is vital for the apparent 'intra-plate' magmatisms. This can be hypothesized with underplating of a small plume of shallow origin, which provided sufficient heat to trigger melting of the isostatically readjusted lower crust for granitic magmas and of metasomatized mantle (melange of subducted lower crust and mantle peridotite) for basic and ultrabasic magmas. Alternatively, the magmatic event was simply initiated by 'internal' heat source from the doubly thickened

radioactive crust by collision, and then aided by the asthenospheric upwelling when the thickened crust underwent extension. We are not able to distinguish the two hypotheses of heat sources, but simultaneous

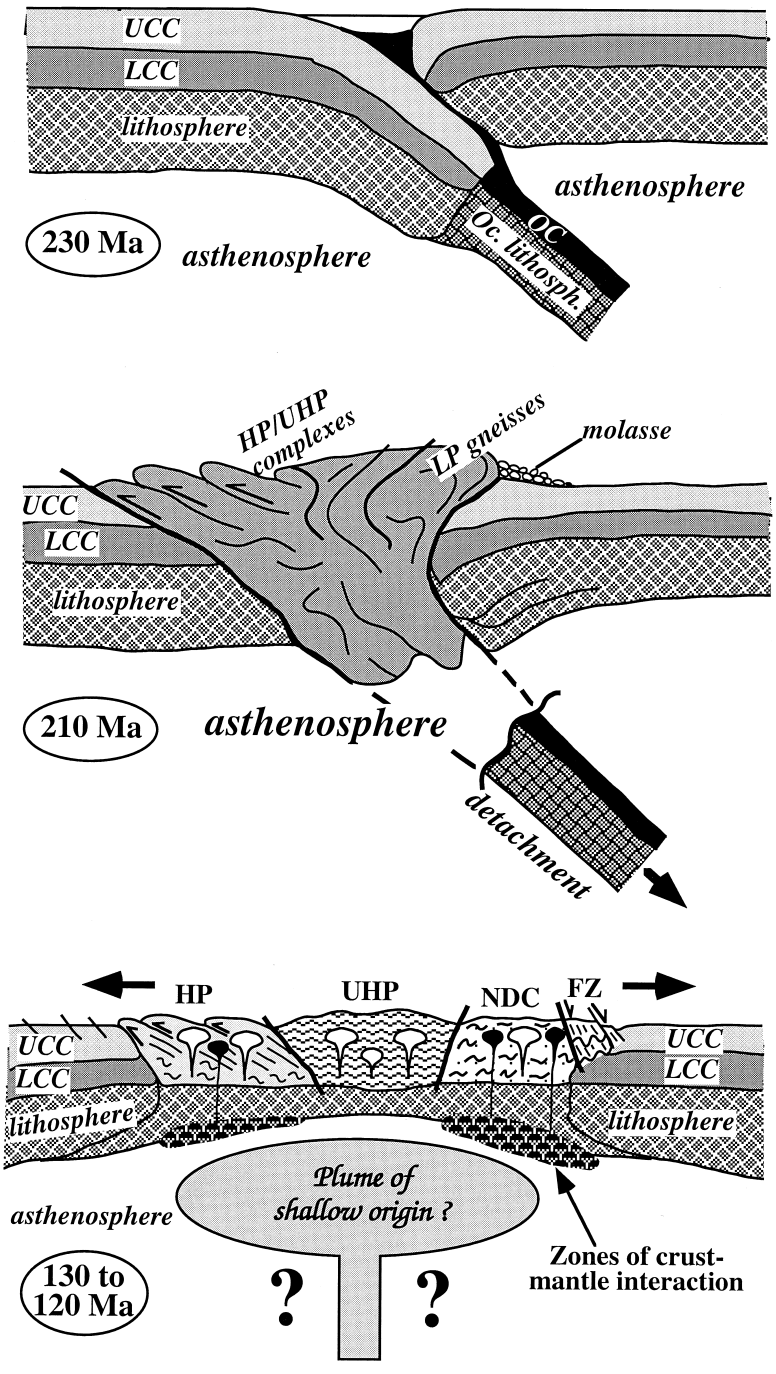

melting of lower crust and metasomatized mantle is essential in this model.

Most recently, Hacker et al. (1998) reported zircon ages with a small range (138–125 Ma) for a viariety of lithological units of the NDC, including an orthogneiss from near Yanzihe, a gabbro, two tonalite intrusions from Yuexi and SW of Changpu, a granitic gneiss from S of Tiantangzhai pluton and an undeformed granite from W of Yinshan. In addition, Xue et al. (1997) also reported two zircon ages of 134 ± 2 and 134 ± 3 Ma for orthogneisses of the NDC. These zircon age data prompted Hacker et al. (1998) to hypothesize that the bulk of the NDC ($> 90\%$) is a Cretaceous magmatic complex, and the pre-Cretaceous 'basement rocks', represented by garnet granulite with minor marble and ultramafic rocks, are only scraps of the Yangtze craton that survived the deep subduction. The new zircon age data are excellent, but their interpretation is very provocative that merits some comments.

If the bulk of the NDC is indeed a Cretaceous magmatic complex, then an interesting question follows: what are the sources (or protoliths) for the vast amount of the magmatic rocks? Our unpublished chemical analyses and literature data show that they are mainly of TTG composition with arc geochemical signature. Modern as well as Archean TTG rocks are believed to be produced by melting of young and hot subducted slabs in subduction zones (Martin, 1986; Defant and Drummond, 1990; Drummond and Defant, 1990). In the case of the post-collisional Dabieshan, the apparent absence of subduction process is incompatible with the formation of the extensive orthogneisses if they were indeed of Cretaceous age.

The zircon age pattern may be favorable for the idea of the Cretaceous magmatic complex. According to Hacker et al. (1998), the Cretaceous granitic magmas were emplaced in two distinct styles: highly deformed orthogneisses with banding and migmatisation and undeformed homogeneous plutons. They noticed that the more deformed plutons tend to have older ages (still Mesozoic) than the less deformed plutons. They suggested that the plutons were intruded during and after an episode of large-scale crustal extension, leading to the contrasting emplacement styles. However, it is still possible that the dominance of Cretaceous zircon ages for the orthogneisses was due to the very strong Cretaceous reheating, leaving only few cores to preserve their Proterozoic age record.

A granitic gneiss, intruded by a Cretaceous (120 Ma) deformed granite at Lanniao, was dated at about 2.0 Ga by SIMS (secondary ion microprobe spectrometry) on zircon grains at Stockholm (Jahn et al., 1999a). Although difficult to verify the reliability of analytical data, Zhou et al. (1995a) reported five zircon ages of 600–800 Ma for granitic gneisses from the NDC and N. Huaiyang Belt including Feidong. Moreover, using the single zircon Pb evaporation technique, Jian et al. (1997) obtained two ages of 2811 (± 27 and ± 29) Ma for a hyperthene–garnet–biotite granulite from Luotian (Huangtuling). They inferred this age to represent the minimum age of the Dabie basement rocks. The above information indicates that the pre-Cretaceous 'basement rocks'

Fig. 11. Tectonic cartoon showing the development of the UHP rocks, crust–mantle interaction and subsequent melting and intrusions of Cretaceous granitic and gabbroic rocks. (a) Northward subduction of the continental crust of the Yangtze craton continued after the initial collision with the Sino-Korean craton, at about 230 Ma. UHP mineral assemblages started to form at mantle depths. (b) Due to its buoyancy the subducted continental lithosphere ceased to descend further, and the eclogitized oceanic lithosphere broke off from it and continued its descent. The buoyant continental lithosphere, particularly its crustal portion, rapidly uplifted and formed the uplifted assemblage including HP/UHP complexes and low pressure gneisses within the UHP complex, at about 210 Ma (in grey, undifferentiated). The uppermost crustal section, little subducted, formed the 'basement gneisses' of the NDC. The break-off of the oceanic lithosphere and following lithospheric extension made room for 'intrusion' of the hotter asthenosphere, which started to 'digest' a part of the subducted continental crust not escaped by rapid uplift. Because the subducted crust was cold and dry, partial melting did not occur immediately. (c) After a long period (≈ 100 Ma) of incubation (crust–mantle interaction), an added heat triggered intense partial melting of the lower crust, producing massive granitic intrusions; meantime, the metasomatized mantle was also subjected melting, producing basic magmas. The heat source is not known, but a small plume of shallow origin is also possible.

may be more abundant than hypothesized by Hacker et al. (1998). Evidently, the controversy on the development of the NDC will persist until more systematic geochronology is done.

5. Conclusions

The present geochemical and Nd–Sr isotopic analyses lead to the following conclusions.

(1) Isotope dating using different techniques (Rb–Sr, Sm–Nd and Ar–Ar) has established that the mafic and ultramafic bodies of the NDC were intruded post-tectonically in early Cretaceous ($\approx$ 120–130 Ma), nearly contemporaneous with the massive emplacement of granitic plutons. They did not form as part of the early Paleozoic arc complex, nor did they undergo UHP metamorphism at about 220 Ma as proposed by earlier workers (Li et al., 1989a,b).

(2) The light rare earth enriched REE patterns for gabbros and diorites, the significant negative Nb anomalies in the spidergrams, as well as the highly negative $\varepsilon_{Nd}(T)$ values (-15 to -20) for all mafic and ultramafic rocks suggest that they were derived from a metasomatised mantle source. For the Jiaoziyan gabbro, an AFC process was probably in effect, leading to non-equibrium of isotopic compositions in constituent minerals. The Sm–Nd age of 240 Ma for Jiaoziyan gabbro reported by Chen et al. (1997) is not confirmed by the present study.

(3) The singular geochemical and isotopic characteristics of the mafic–ultramafic rocks provide a strong argument for a post-collisional interaction between the Triassic subducted ancient crust (Yangtze craton) and the mantle peridotite (asthenosphere). Partial melting of such enriched metasomatized mantle produced the basic and ultrabasic magmas, in response to the same thermal pulse that was responsible for the massive Cretaceous granitic intrusions and resetting of some isotopic clocks in UHP metamorphic rocks.

(4) When dealing with the problems of continental growth and destruction, three recycling processes have been commonly assumed: injection of sediments in subduction zones, delamination of lower continental crust (Arndt and Goldstein, 1989; Kay and Kay, 1991) or of continental lithosphere (McKenzie and O'Nions, 1983). We advocate that a fourth process, the digestion of deeply subducted continental blocks in mantle peridotites, as a potential way of recycling the continental crust.

Acknowledgements

Fuyuan Wu is most grateful to the laboratory staff for the tutoring of analytical techniques during his stay in Rennes (9/1995–9/1996). Bolin Cong of the Chinese Academy of Sciences kindly invited BmJ for field work and sampling in the Dabie and Su-Lu regions during 1992–1995. We have benefitted from a new cooperative work with the Chinese Academy of Geological Sciences (leader: Dunyi Liu), and field guidance of Jiafu Tang of the Anhui Institute of Geology in 1996. We thank Jean Cornichet, Joël Macé, Nicole Morin, Odile Henin, and Martine Le Coz-Bouhnik for assistance in various phases of analytical work. Jean de Bremond d'Ars gave a quick instruction on magma cooling process. Constructive comments were provided by J.G. Liou (Stanford), Nick Arndt (Rennes) and journal reviewers Brad Hacker and Leonid Neymark. The present research on continental subduction and UHP metamorphism in central China has been supported by the following grants: 'Allocation Spécifique-DGRT' of French Ministry of Education (1995), DBT II (1996) and 'Intérieur de la Terre' (1997) of INSU-CNRS. This is INSU contribution no. 174. Ching-Hua Lo acknowledges a financial support from NSC of Taiwan. *[MB]*

Appendix A. Petrographic description

A.1. BJ93-10

Very coarse-grained hornblende gabbro, from Shacun Locality #1. It shows no trace of metamorphism. Porphyritic and poikilitic texture with large amphibole crystals ($\approx$ 1 cm size, up to 2.5 cm) enclosing numerous inclusions of Cpx, Plag, Ap, Opq and Sph. The matrix assemblage is medium-grained (mean size $\approx$ 2 mm; mainly 1–3 mm), consisting of Plag, Cpx and Sph. Plagioclase shows albite twinning and zoning; some altered to granular saussurite and some to very fine-grained clay minerals. Cpx shows conversion to green Hb in some cases, and occurs as inclusions in Plag in others. Generally, inclusion Cpx appears less altered than

matrix Cpx, and both are of the same size. Opaques include magnetite and ilmenite, with ilmenite altered to leucoxene showing well-aligned sphene. Secondary chlorite present. Because of the poikilitic nature of amphibole, the isotopic analysis of the Hb fraction in Table 3 does not represent a pure hornblende analysis.

A.2. BJ93-11

Porphyritic diorite, from Shacun Locality #1. Phenocrystals comprise plagioclase and subordinate green biotite. Plag is prismatic or lath-shaped, euhedral to subhedral. The average size is about 4 mm long, with some up to 8 mm. It shows twinning and zoning; alteration is common in crystal margins. The matrix is composed of Plag, Hb, Bio, K-spar, Opq and trace amounts of sphene and apatite. Hornblende is much more abundant than biotite among colored minerals, and is partially converted to biotite. The proportion of phenocrysts to matrix is about 25/75. The mineral assemblage shows no metamorphism, deformation or preferred orientation of phases, but some alteration.

A.3. BJ93-21

Gabbro or gabbro-norite, from Shacun Locality #2. Principal phases include green Cpx, Opx, Plag, brown to green Hb, Bio, and highly altered Ol. Accessories include Opq and zircon. Plagioclase shows twinning and some sericitisation. Poikilitic texture with large Hb enclosing numerous inclusions of Cpx, Opx, Opq, and Ol. Plagioclase rarely occurs as inclusion. Twinning in Cpx is common, but not in Opx. Cpx is subhedral to anhedral, and it shows no zoning. Some pale-green Cpx is converted to fan-shaped fine fibrous bundles (micaceous?). Partial conversion of hornblende to biotite is observed. Olivine is highly altered and released magnetite along grain boundaries and cracks.

A.4. BJ93-22

Quartz diorite, from Shacun Locality #2. Light-colored, with plagioclase ($=50\%$) and quartz ($\approx 20\%$) dominating the assemblage. Plag is euhedral to subhedral, showing twinning and oscillatory zoning, and occasionally containing abundant tiny grains of apatite, zircon and sphene. Some plagioclase crystals are very big, up to 1.5 cm long; and some show saussuritisation and sericitisation. Colored minerals are mainly composed of green Hb and brown Bio in about equal proportion. Accessory phases include zircon, opaques, apatite and sphene. Chlorite formed by biotite alteration.

A.5. BJ93-23

Amphibole diorite, from Shacun Locality 2 and from the same block as BJ93-22. The phase assemblage is similar to BJ93-22, but its proportion of amphibole is much higher, leading to the high MgO content. Colored minerals represents ≈ 60–65%. Light-green Hb is euhedral to subhedral, some are twinned. The inner part of green Hb is often brown-colored, and in many cases, conversion into biotite is evident. Hb contains numerous inclusions, thus separation of pure Hb fraction cannot be achieved. Biotite occurs only inside amphibole crystals by Hb conversion. It appears that the conversion of Hb produced biotite and small sphene grains oriented along cleavage. Light-colored phases include Plag, Qtz and K-spar, in descending order of abundance. Accessory minerals are apatite (some are as large as 3×1 mm^2) and interstitial sphene. This rock was probably formed by amphibole accumulation from a dioritic liquid, forming the complementary part of BJ93-23.

A.6. BJ95-03

Olivine pyroxenite, from Zhujiapu. Coarse-grained (average grain size ≈ 3 mm, varying from 1–8 mm), composed predominantly of colored minerals. Olivine ($\approx 10\%$) is highly fractured, but not much serpentinised. Minute opaque grains occur in fractures of olivine. Cpx is most distinguished by its diallage texture. Opx shows pleochroism and apparent diallage with parallel alignments of opaque phases. Some Opx enclose Cpx crystals. Cpx + Opx represent about 60–65%. Brown Hb ($\approx 25\%$) contains fine-grained dark brown minerals (iron oxides?) formed along and across cleavage planes. Some carbonate crystals are developed within Hb. Accessory minerals are opaques and, very rarely, biotite (few grains). No plagioclase is observed in this thin section, but it is present in very small quantity in the other portion of the sample which was subjected to crushing and mineral separation.

A.7. BJ95-04

Fine-grained gabbro (or dioritic gabbro), from Zhujiapu. This is a dike cutting the above olivine pyroxenite. Average grain size ≈0.5 mm. Mafic minerals (=40%) include mainly green Hb and brown Bio in about equal proportion. Hornblende is significantly coarser than biotite. Rare residual Cpx is observed, being surrounded by green Hb. Small amount of epidote also occur. The non-colored assemblage (≈60%) is almost entirely composed of plagioclase; quartz and K-spar (?) constitute the remainder. Accessory phases are abundant (≈2%), including apatite, sphene, opaques, zircon and epidote.

A.8. 95DB-13P

Gabbro (or gabbronorite), from inner part of the Jiaoziyan body. Massive and medium-grained, it contains 40–45% Plag, 30–35% Cpx, 10–15% Opx, 5% Bio, and minor ilmenite, magnetite, and trace apatite. Plagioclase (0.5–4 mm) is coarser than pyroxenes (0.2–1.5 mm); the smaller pyroxenes often occur along the grain boundaries of the larger tabular plagioclase. Deformation twins and zoning are common in plagioclase. Some coarse plagioclase grains include oriented dark greenish brown rods. The two pyroxenes mostly occur as aggregates. Augite is clouded with amphibole patches and very fine grained inclusions, and occasionally with oriented brown lamellae (orthopyroxene?). Orthopyroxene contains oriented brown platelets (spinel?) and dark needles. Brown (Ti-bearing) biotite is interstitial; it mantles pyroxenes, plagioclase, and opaques. Opaques appear to surround pyroxenes. Rare apatite occurs as blocky grains or needles in plagioclase and biotite.

References

Amelin, Y.V., Neymark, L.A., Ritsk, E.Y., Nemchin, A.A., 1996. Enriched Nd–Sr–Pb isotopic signatures in the Dovyren layered intrusion (eastern Siberia, Russia): evidence for source contamination by ancient upper-crustal material. Chem. Geol. 129, 39–69.

Ames, L., Tilton, G.R., Zhou, G., 1993. Timing of collision of the Sino-Korean and Yangtze cratons: U–Pb zircon dating of coesite-bearing eclogites. Geology 21, 339–342.

Ames, L., Zhou, G., Xiong, B., 1996. Geochronology and isotopic character of high-pressure metamorphism with implications for collision of the Sino-Korean and Yangtze cratons, central China. Tectonics 15, 472–489.

Anderson, T.B., Jamtveit, B., Dewey, J.F., Swensson, E., 1991. Subduction and eduction of continental crust: major mechanisms during continent–continent collision and orogenic extensional collapse, a model based on the south Norwegian Caledonides. Terra Nova 3, 303–310.

Arndt, N.T., Goldstein, S.L., 1989. An open boundary between lower continental crust and mantle: its role in crust formation and crustal recycling. Tectonophysics 161, 201–212.

Avigad, D., 1992. Exhumation of coesite-bearing rocks in the Dora Maira massif (western Alps, Italy). Geology 20, 947–950.

Chavagnac, V., Jahn, B.M., 1996. Coesite-bearing eclogites from the Bixiling Complex, Dabie Mountains, China: Sm–Nd ages, geochemical characteristics and tectonic implications. Chem. Geol. 133, 29–51.

Chen, J.F., Jahn, B.M., 1998. Crustal evolution of southeastern China: Nd and Sr isotopic evidence. Tectonophysics 284, 101–133.

Chen, T.Y., Niu, B.G., Liu, Z.G., 1991. Isotope age study of the Yanshanian magmatism and metamorphism in Dabieshan and its geological significance. Acta Geosci. Sinica 12, 329–335, (in Chinese).

Chen, J.F., Xie, Z., Liu, S.S., 1995. ^{40}Ar–^{39}Ar and fission track cooling ages of the Dabie orogenic belt. Chin. Sci. B 25, 1086–1092.

Chen, D.G., Wu, Y.B., Xia, Q.K., Zhi, X.C., Wang, Y.X., Yang, J.D., 1997. Sm–Nd age and Nd isotopic characteristics of the Jiaoziyan gabbroic intrusion. Acta Geosci. Sinica 18, 9–11.

Chen, N.S., Sun, M., You, Z.D., Malpas, J., 1998. Well-preserved garnet growth zoning in granulite from the Dabie Mountains, central China. J. Metamorphic Geol. 16, 213–222.

Chopin, C., 1984. Coesite and pure pyrope in high grade blueschists of the western Alps: a first record and some consequences. Contrib. Mineral. Petrol. 86, 107–118.

Condie, K., 1993. Chemical composition and evolution of the upper continental crust: contrasting results from surface samples and shales. Chem. Geol. 104, 1–37.

Cong, B. (Ed.), 1996. Ultrahigh-pressure metamorphic rocks in the Dabieshan–Sulu region of China. Science Press Beijing, China and Kluwer Acad. Publ., Dordrecht, 224 pp.

Davis, J.H., von Blanckenburg, F., 1995. Slab breakoff: a model of lithosphere detachment and its test in the magmatism and deformation of collisional orogens. Earth Planet. Sci. Lett. 129, 85–102.

Defant, M.J., Drummond, M.S., 1990. Derivation of some modern arc magmas by melting of young subducted lithosphere. Nature 347, 662–665.

DePaolo, D.J., 1981. Trace element and isotopic effects of combined wallrock assimilation and fractional crystallization. Earth Planet. Sci. Lett. 53, 189–202.

Drummond, M.S., Defant, M.J., 1990. A model for trondhjemite–tonalite–dacite genesis and crustal growth via slab melting: Archean to modern comparisons. J. Geophys. Res. 95, 21503–21521.

Eide, E., 1995. A model for the tectonic history of HP and UHPM

regions in east central China. In: Coleman, R.G., Wang, X.M. (Eds.), Ultrahigh-Pressure Metamorphism. Cambridge Press, pp. 391–426.

Hacker, B.R., Wang, Q.C., 1995. Ar/Ar geochronology of ultrahigh-pressure metamorphism in central China. Tectonics 14, 994–1006.

Hacker, B.R., Ratschbacher, L., Webb, L., Dong, S.W., 1995. What brought them up? Exhumation of the Dabie Shan ultrahigh-pressure rocks. Geology 23, 743–746.

Hacker, B.R., Wang, X., Eide, E.A., Ratschbacher, L., 1996. The Qinling–Dabie ultrahigh-pressure collisional orogen. In: Yin, A., Harrison, T.M. (Eds.), The Tectonic Evolution of Asia. Cambridge Univ. Press, UK, pp. 345–370.

Hacker, B.R., Ratschbacher, L., Webb, L., Ireland, T., Walker, D., Dong, S.W., 1998. U/Pb zircon ages constrain the architecture of the ultrahigh-pressure Qinling–Dabie orogen, China. Earth Planet. Sci. Lett. 161, 215–230.

Jahn, B.M., 1998. Geochemical and isotopic characteristics of UHP eclogites and ultramafic rocks of the Dabie orogen: implications for continental subduction and collisional tectonics. In: Hacker, B., Liou, J.G. (Eds.), When Continents Collide: Geodynamics and Geochemistry of Ultrahigh-Pressure Rocks. Kluwer Acad. Publishers, Dordrecht, The Netherlands.

Jahn, B.M., Zhang, Z.Q., 1984. Archean granulite gneisses from eastern Hebei Province, China: rare earth geochemistry and tectonic implications. Contrib. Mineral. Petrol. 85, 224–243.

Jahn, B.M., Cornichet, J., Henin, O., Le Coz-Bouhnik, M., Cong, B.L., 1994. Geochemical and isotopic investigation of ultrahigh pressure (UHP) metamorphic terranes in China: Su-Lu and Dabie complexes. Stanford Workshop on 'Ultrahigh-P metamorphism and tectonics', pp. A71–A74.

Jahn, B.M., Cornichet, J., Cong, B.L., 1995. Crustal evolution of the Qinling–Dabie orogen: isotopic and geochemical constraints from coesite-bearing eclogites of the Su-Lu and Dabie terranes, China. Chin. Sci. Bull. Vol. 40, 116–119.

Jahn, B.M., Cornichet, J., Cong, B.L., Yui, T.F., 1996. Ultrahigh-ε_{Nd} eclogites from an ultrahigh pressure metamorphic terrane of China. Chem. Geol. 127, 61–79.

Jahn, B.M., Potel, S., Villa, I.M., Whitehouse, M.J., Andriessen, P., 1999a. Age and isotopic constraints to the architecture of the Dabie UHP metamorphic terrane, China. Abs. EUG-10, in press.

Jahn, B.M., Fan, Q.C., Yang, J.J., Henin, O., 1999b. Genesis of the Maowu pyroxenite–eclogite body from the UHP metamorphic terrane of Dabieshan: chemical and isotopic constraints and tectonic implications, to be submitted to Chem. Geol.

Jian, P., Zhang, Z.C., Zhu, J.P., Lu, H., Yang, W.R., Han, Y.Q., Wang, L.S., 1997. The Dabie basement is older than 2800 Ma: evidence from the zircon age of granulite from Huangtuling. Acta Geosci. Sinica 18, 65–67.

Kay, R.W., Kay, S.M., 1991. Creation and destruction of lower continental crust. Geol. Rundsch. 80, 259–278.

Lanphere, M.A., Dalrymple, G.B., 1978. The use of $^{40}Ar/^{39}Ar$ data in evaluation of disturbed K–Ar systems. US Geological Survey Open-file Report 78-701, pp. 241–143.

Le Roux, A.P., 1986. Geochemical correlation between southern African kimberlites and south Atlantic hotspots. Nature 324, 243–245.

Li, Z.X., 1994. Collision between the north and south China blocks: a crustal-detachment model for suturing in the region east of the Tanlu fault. Geology 22, 739–742.

Li, S., Hart, S.R., Zheng, S., Liou, D., Zhang, G., Guo, A., 1989a. Timing of collision between the north and south China blocks —the Sm–Nd isotopic age evidence. Sci. China (Ser. B) 32, 1391–1400.

Li, S., Ge, N.J., Liu, D., Zhang, Z., Ye, X., Zheng, S., Peng, C., 1989b. The Sm–Nd isotopic age of C-type eclogite from the Dabie Group in the northern Dabie Mountians and its tectonic implication. Chin. Sci. Bull. 34, 1623–1628.

Li, S., Xiao, Y., Liu, D., Chen, Y., Ge, N., Zhang, Z., Sun, S.S., Cong, B., Zhang, R., Hart, S.R., 1993. Collision of the north China and Yangtze blocks and formation of coesite-bearing eclogites: timing and processes. Chem. Geol. 109, 89–111.

Li, S., Wang, S., Chen, Y., Liu, D., Qiu, J., Zhou, H., Zhang, Z., 1994. Excess argon in phengite from eclogite: evidence from the dating of eclogite minerals by the Sm–Nd, Rb–Sr and $^{40}Ar/^{39}Ar$ methods. Chem. Geol. 112, 343–350.

Liou, J.G., Zhang, R.Y., Wang, X.M., Eide, E.A., Ernst, W.G., Maruyama, S., 1996. Metamorphism and tectonics of high-pressure and ultrahigh-pressure belts in the Dabie–Su-Lu region, China. In: Yin, A., Harrison, T.M. (Eds.), The Tectonic Evolution of Asia. Cambridge Univ. Press, UK, pp. 300–344.

Liou, J.G., Zhang, R.Y., Ernst, W.G., 1997. Lack of fluid during ultrahigh-P metamorphism in the Dabie–Su-Lu region, eastern China. Proc. 30th Int'l Geol. Congr. Vol. 17, Part II, VSP 1997, pp. 141–155.

Liu, X., Hao, J., 1989. Structure and tectonic evolution of the Tongbai–Dabie range in the east Qinling collisional belt. Tectonics 8, 637–645.

Lo, C.H., Lee, C.Y., 1994. $^{40}Ar/^{39}Ar$ method of K–Ar age determination of geological samples using Tsing-Hua Open-Pool (THOPR) reactor. J. Geol. Soc. China 37, 1–22.

Ludwig, K.R., 1990. ISOPLOT: A plotting and regression program for radiogenic isotope data, for IBM-PC compatible computers, Version 2.12. USGS Open-file report 88-557, 31 pp.

Martin, H., 1986. Effect of steeper Archean geothermal gradient on geochemistry of subduction zone magmas. Geology 14, 753–756.

Maruyama, S., Liou, J.G., Zhang, R., 1994. Tectonic evolution of the ultrahigh-pressure (UHP) and high-pressure (HP) metamorphic belts from central China. The Island Arc 3, 112–121.

Masuda, A., Nakamura, N., Tanaka, T., 1973. Fine structures of mutually normalized rare earth patterns of chondrites. Geochim. Cosmochim. Acta 37, 239–248.

Mattauer, M., Matte, Ph., Malavieille, J., Tapponnier, P., Maluski, H., Xu, Z.Q., Lu, Y.L., Tang, Y.Q., 1985. Tectonics of the Qinling Belt: build-up and evolution of eastern Asia. Nature 317, 496–500.

Mattauer, M., Matte, Ph., Maluski, H., Xu, Z.Q., Zhang, Q.W., Wang, Y.M., 1991. La limite Chine du Nord–Chine du Sud au Paléozoïque et au Trias. Nouvelles données structurales et radiométriques dans le massif de Dabie-Shan (chaîne des Qinling). C. R. Acad. Sci. Paris 312, 1227–1233.

McKenzie, D., O'Nions, R.K., 1983. Mantle reservoirs and ocean island basalts. Nature 301, 229–231.

Michard, A., Chopin, C., Henry, C., 1993. Compression versus extension in the exhumation of the Dora–Maira coesite-bearing unit, western Alps, Italy. Tectonophysics 221, 173–193.

Odin, G.S., 35 collaborators, 1982. Interlaboratory standards for dating purposes. In: Odin, G.S. (Ed.), Numerical Dating in Stratigraphy, Wiley.

Okay, A.I., 1993. Petrology of a diamond and coesite-bearing metamorphic terrain: Dabie Shan, China. Eur. J. Mineral. 5, 659–675.

Okay, A.I., Sengör, A.M.C., 1992. Evidence for intracontinental thrust-related exhumation of ultrahigh-pressure rocks in China. Geology 20, 411–414.

Okay, A.I., Sengör, A.M.C., Satir, M., 1993. Tectonics of an ultrahigh-pressure metamorphic terrane: the Dabieshan/Tongbaishan orogen, China. Tectonics 12, 1320–1334.

RGS (Regional Geological Survey) Anhui, 1987. Geology of Anhui Provinve, Geology Publ., Beijing, 721 pp. and maps (in Chinese, with 70 pp. of English summary).

Rowley, D.B., Xue, F., Tucker, R.D., Peng, Z.X., Baker, J., Davis, A., 1997. Ages of ultrahigh pressure metamorphism and protolith orthogneisses from the eastern Dabie Shan: U/Pb zircon geochronology. Earth Planet. Sci. Lett. 151, 191–203.

Rudnick, R.L., Fountain, D.M., 1995. Nature and composition of the continental crust: a lower crustal perspective. Rev. Geophys. 33, 267–309.

Sun, S.S., McDonough, W.F., 1989. Chemical and isotopic systematics of oceanic basalts: implications for mantle composition and processes. In: Saunders, A.D., Norry, M.J. (Eds.), Magmatism in the Ocean Basins. Geol. Soc. Special Publications, no. 42, pp. 313–345.

Tatsumi, Y., Eggins, S., 1995. Subduction Zone Magmatism. Blackwell Science, Cambridge, MA, USA, 211 pp.

Taylor, H.P. Jr., 1980. The effects of assimilation of country rocks by magmas on $^{18}O/^{16}O$ and $^{87}Sr/^{86}Sr$ systematics in igneous rocks. Earth Planet. Sci. Lett. 47, 243–254.

Taylor, S.R., McLennan, S.M., 1985. The Continental Crust: Its Composition and Evolution. Blackwell, 312 pp.

Tsai, C.H., Liou, J.G., 1997. Inferred ultrahigh-pressure eclogitic metamorphism in the north Dabie complex, central-eastern China. Geol. Soc. Am. Abstr. With Program 29, A–336.

Tsai, C.H., Liou, J.G., Ernst, W.G., 1998. Petrological characterisation of Raobazhai metaperidotites, north Dabie complex, east-central China. WPGM abstract, EOS Supplement, vol. 79, p. W128.

Wang, Q.C., 1996. Tectonic implication of UHP rocks from the Dabie Mountains. Sci. China (Ser. D) 39, 311–318.

Wang, X.M., Liou, J.G., 1991. Regional ultrahigh-pressure coesite-bearing eclogite terrane in central China: evidence from country rocks, gneiss, marble and metapelite. Geology 19, 933–936.

Wang, X.M., Zhang, R.Y., Liou, J.G., 1995. UHPM terrane in east central China. In: Coleman, R.G., Wang, X.M. (Eds.), Ultrahigh Pressure Metamorphism. Cambridge Univ. Press, Cambridge, pp. 356–390.

Wang, Q.C., Zhai, M.G., Cong, B.L., 1996. Regional geology. In: Cong, B.L. (Ed.), Ultrahigh-Pressure Metamorphic Rocks in the Dabieshan–Sulu Region of China. Science Press, Beijing and Kluwer Acad. Publ., Dordrecht, pp. 8–26.

Xie, Z., Chen, J.F., Zhou, T.X., Zhang, X., 1996. Nd isotopic compositions of metamorphic and granitic rocks from Dabie orogen and their geological significance. Acta Petrol. Sinica 12, 401–408.

Xu, S., Jiang, L.L., Liu, Y.C., Zhang, Y., 1992. Tectonic framework and evolution of the Dabie Mountains in Anhui, eastern China. Acta Geol. Sinica 5, 221–238.

Xu, S., Liu, Y.C., Jiang, L.L., Su, W., Ji, S.Y., 1994. Tectonic framework and evolution of Dabieshan. Science Publishing, Beijing, 175 pp. (in Chinese, with 8 pp. of English summary).

Xu, S., Jiang, L.L., Liu, Y.C., Su, W., Ji, S.Y., 1995. The characteristic structures and lithological units of Dabieshan: their formation and evolution. Anhui Inst. Geology, 107 pp. (in Chinese).

Xue, F., Rowley, D.B., Yucker, R.D., Peng, Z.X., 1997. U–Pb zircon ages of granitoid rocks in the north Dabie complex, eastern Dabie Shan, China. J. Geol. 105, 744–753.

Yin, A., Nie, S., 1993. An indentation model for the north and south China collision and the development of the Tanlu and Honam fault systems, eastern Asia. Tectonics 12, 801–813.

York, D., 1969. Least-squares fitting of a straight line with correlated errors. Earth Planet. Sci. Lett. 5, 320–423.

Zhai, M., Cong, B., Zhang, Q., Wang, Q., 1994. The northern Dabieshan terrain: a possible Andean-type arc. Int. Geol. Rev. 36, 867–883.

Zhang, L.G., Wang, K.F., Chen, Z.S., Liu, J.X., 1995. Block geology of eastern Asian lithosphere—isotope geochemistry and dynamics of upper mantle, basement and granites. Science Press, Beijing, 252 pp. (in Chinese).

Zhang, R.Y., Liou, J.G., Tsai, C.H., 1996. Petrogenesis of a high-temperature metamorphic terrane: a new tectonic interpretation for the north Dabieshan, central China. J. Metamorphic Geol. 14, 319–333.

Zheng, W.Z., Liu, G.L., Wang, X.W., 1991. New information on the Archean eon for the Kongling group in northern Huangling anticline, Hubei. Bull. Yichang Inst. Geol. Miner. Res. 16, 97–106.

Zhou, T.X., Chen, J.F., Li, X.M., Chen D.G., Zhi, X.C., 1992. Geochemical characteristics and petrogenesis of the Xianhongdian alkaline complex, Anhui Province. In: Li, J.L. (Ed.), Lithospheric Structure and Evolution in SE China. China Sci. Tech. Press., pp. 182–192 (in Chinese).

Zhou, C.T., Tang, J.F., Gao, T.S., Lu, R.K., 1995a. The formation and geochronology of the basement gneisses of the Dabie Mountains. Geol. Anhui 5, 29–40.

Zhou, T.X., Chen, J.F., Zhang, X., 1995b. Geochemical study of the granite-syenite belt in the N. Huaiyang region and its tectonic significance. Geol. Rev. 41, 144–151.

Zhou, T.X., Li, X., Zhang, X., Wei, G., Pan, G., Chen, J., 1995c. A lead isotopic study of alkali intrusion in the N. Huaiyang region. J. China Univ. Sci. Technol. 25, 467–473.